

THESIS FOR THE DEGREE OF DOCTOR OF PHILOSOPHY

Operando X-ray Absorption Spectroscopy Studies of Methane
Oxidation Catalysts

JOHAN NILSSON



CHALMERS

Department of Chemistry and Chemical Engineering
CHALMERS UNIVERSITY OF TECHNOLOGY

Göteborg, Sweden 2017

Operando X-ray Absorption Spectroscopy Studies of Methane Oxidation Catalysts
JOHAN NILSSON
ISBN 978-91-7597-660-0

© JOHAN NILSSON, 2017

Doktorsavhandlingar vid Chalmers tekniska högskola
Ny serie nr. 4341
ISSN 0346-718X

Department of Chemistry and Chemical Engineering
Chalmers University of Technology
SE-412 96 Göteborg
Sweden
Telephone: +46 (0)31-772 1000

Cover:
Cartoon illustrating catalytic methane oxidation over a solid catalyst, overlaid with K edge XAFS spectrum of metallic Pd.

Chalmers Reproservice
Göteborg, Sweden 2017

ABSTRACT

Operando spectroscopy is an experimental method in catalysis that combines measurements of catalytic activity and selectivity with simultaneous in situ spectroscopic characterization of the catalyst. Since the structure and composition of the catalyst are probed under reaction conditions, the method can provide valuable information to elucidate the mechanism of the studied reaction. In this thesis, operando spectroscopy has been performed using X-ray absorption fine structure (XAFS) as an in situ characterization technique to study catalysts during the total oxidation of methane. Methane is a strong greenhouse gas and catalytic oxidation can be used, for example, to remove uncombusted methane from the exhausts of vehicles fueled with natural gas or biogas.

Palladium is the most active metal for the total oxidation of methane, but the oxidation state of palladium can change rapidly during reaction conditions, which has an effect on the catalytic activity. Time-resolved XAFS was used to investigate Pd/Al₂O₃ catalysts under transiently changing reaction conditions for methane oxidation, by performing oxygen pulse-response experiments, so the conditions periodically change from net-reducing to net-oxidizing. Simultaneously, the outlet concentrations of reactants and products were monitored with mass spectrometry. The XAFS data show that palladium in the catalyst is readily reduced and oxidized when the feed gas composition is changed from reducing to oxidizing. The highest activity for methane oxidation is found over bulk-oxidized palladium (PdO), while surface oxidized palladium in comparison is less active. Similar experiments were also performed for a Pd/CeO₂ catalyst. Compared to the alumina supported catalyst, palladium supported on CeO₂ is oxidized more rapidly in an oxidizing atmosphere, and is reduced at a slower rate in a reducing atmosphere. This shows that CeO₂ is able to stabilize Pd in the oxidized state which, could be beneficial for the methane oxidation activity.

Moreover, methane oxidation under cycling conditions was investigated for bimetallic Pd–Pt/Al₂O₃ catalysts. Pd–Pt catalysts have attracted interest due their higher long-term stability compared to Pd-only catalysts. In our studies we found that the calcination temperature during catalyst preparation is of high importance for the morphology of the catalysts. For catalysts calcined at 500 °C, Pd and Pt are not alloyed but are found as separate Pd and Pt nanoparticles. However, for catalysts calcined at 800 °C alloyed Pd–Pt nanoparticles are found as well as monometallic Pd nanoparticles. The methane conversion was higher over the alloyed Pd–Pt nanoparticles calcined at 800 °C. In similarity to the Pd-only catalyst, high activity for methane oxidation is connected to a high amount of oxidized palladium in the catalyst. Although XAFS is only available at synchrotron light sources, the ability to investigate the active phase of catalysts with high time resolution, under reaction conditions, makes it a highly useful technique in catalysis research.

Keywords: heterogeneous catalysis, methane oxidation, palladium, operando spectroscopy, XAS, XAFS

LIST OF PUBLICATIONS

This thesis is based on the following appended papers:

- Paper I** J. Nilsson, P.-A. Carlsson, S. Fouladvand, N. M. Martin, J. Gustafson, M. A. Newton, E. Lundgren, H. Grönbeck, and M. Skoglundh. Chemistry of Supported Palladium Nanoparticles during Methane Oxidation. *ACS Catalysis*, **5** (2015), 2481–2489.
- Paper II** J. Nilsson, P.-A. Carlsson, N. M. Martin, E. C. Adams, G. Agostini, H. Grönbeck, and M. Skoglundh. Methane Oxidation Over Pd/Al₂O₃ Under Rich/Lean Cycling Followed by Operando XAFS and Modulation Excitation Spectroscopy. *Journal of Catalysis*, **356** (2017), 237–245.
- Paper III** J. Nilsson, P.-A. Carlsson, N. M. Martin, P. Velin, D. Motta Meira, H. Grönbeck, and M. Skoglundh. Oxygen Step Response Experiments for Methane Oxidation over Pd/Al₂O₃: An In Situ XAFS study. *Submitted to Catalysis Communications* (2017).
- Paper IV** N. M. Martin, J. Nilsson, M. Skoglundh, E. C. Adams, X. Wang, P. Velin, G. Smedler, A. Raj, D. Thompsett, H. H. Brongersma, T. Grehl, G. Agostini, O. Mathon, S. Carlson, K. Norén, F. J. Martinez-Casado, Z. Matej, O. Balmes, and P.-A. Carlsson. Characterization of Surface Structure and Oxidation/Reduction Behaviour of Pd-Pt/Al₂O₃ Model Catalysts. *Journal of Physical Chemistry C*, **120** (2016), 28009–28020.
- Paper V** N. M. Martin, J. Nilsson, M. Skoglundh, E. C. Adams, X. Wang, G. Smedler, A. Raj, D. Thompsett, G. Agostini, S. Carlson, K. Norén, and P.-A. Carlsson. Study of Methane Oxidation over Alumina Supported Pd–Pt Catalysts using Operando DRIFTS/MS and In Situ XAS techniques. *Catalysis, Structure & Reactivity*, **3** (2017), 24–32.
- Paper VI** J. Nilsson, P.-A. Carlsson, H. Grönbeck, and M. Skoglundh. First Principles Calculations of Palladium Nanoparticle XANES Spectra. *Topics in Catalysis*, **60**, (2017), 283–288.

MY CONTRIBUTIONS TO THE PUBLICATIONS

Paper I

I performed all the data analysis, interpreted the results together with my co-authors, wrote the first draft of the manuscript, and was responsible for the submission of the manuscript.

Paper II

I participated in the preparation of the catalysts and the collection of experimental data. I performed all the data analysis, interpreted the results together with my co-authors, wrote the first draft of the manuscript, and was responsible for the submission of the manuscript.

Paper III

I participated in the preparation of the catalysts and the collection of experimental data. I performed all the data analysis, interpreted the results together with my co-authors, and wrote the first draft of the manuscript.

Paper IV

I participated in the collection and analysis of the XAFS data, and interpreted the results together with my co-authors.

Paper IV

I participated in the collection and analysis of the XAFS data, and interpreted the results together with my co-authors.

Paper VI

I performed all the calculations, interpreted the results together with my co-authors, wrote the first draft of the manuscript, and was responsible for the submission of the manuscript.

CONTENTS

Abstract	i
List of Publications	iii
My contributions to the publications	iv
Contents	v
1 Introduction	1
1.1 Unravelling the catalyst structure-activity relationship	2
1.2 Objectives	3
2 Operando Spectroscopy	4
2.1 In situ characterization	4
2.2 Transient kinetic measurements	7
3 X-ray absorption fine structure	9
3.1 X-ray absorption spectra	9
3.2 EXAFS analysis	12
3.3 Multiple-scattering XAFS calculations	14
3.4 Modulation excitation spectroscopy	15
4 Model catalysts in catalysis research	18
4.1 Scaling back complexity from realistic catalysts	18
4.2 Synthesis and characterization	19
5 Methane oxidation over Pd catalysts	22
5.1 Oxidation state of Pd during methane oxidation	24
5.2 Support effects	34
5.3 Bimetallic Pt-Pd catalysts	35
5.4 Simulated XAFS spectra from first principles	41
6 Conclusions and Outlook	43
6.1 Next steps	43
6.2 Outlook	44
7 Acknowledgements	46
References	47

Chapter 1

Introduction

One key challenge for a sustainable development is to reduce the emissions of greenhouse gases in the transport sector. This has led to an increased interest in alternative fuels to supplement traditional petroleum fuels such as petrol and diesel. One such alternative fuel is natural gas, which is a gaseous fossil fuel found abundantly in the crust of the earth.

Natural gas consists primarily of methane, which is the simplest hydrocarbon, but also contains longer hydrocarbons such as ethane and butane. A small percentage of other gases such as hydrogen, carbon dioxide, and hydrogen sulfide are often also present. As a fuel, natural gas burns cleanly with low emissions of nitrogen oxides (NO_x) and particulate matter, which helps to minimize the impact on the local environment [1]. Natural gas is also the fossil fuel with the highest hydrogen-to-carbon ratio, which means that combustion of methane results in the lowest emissions of carbon dioxide (CO_2) per unit of energy released. Replacing other fossil fuels with natural gas has been suggested as strategy to lower CO_2 emissions to the atmosphere, and reduce long-term climate change [2]. Furthermore, natural gas can be easily substituted with biogas, which is a methane-rich fuel produced from biological feedstocks. Biogas can be mixed with natural gas in any proportion and is fully compatible with existing natural gas technologies, which means that biogas can be introduced in the current supply of fuel as production allows. This makes natural gas technology attractive as a bridge between fossil and renewable fuels [3].

In the production, transportation and use of natural gas or biogas, it is critical that emissions of methane to the atmosphere are minimized. This is because methane is a strong greenhouse gas, with a global warming potential 86 over 20 years (global warming potential is measured relative to carbon dioxide, which has a standardized value of unity) [4]. When methane is used as a fuel in a vehicle, to power an internal combustion engine, ideally all methane would be combusted to form carbon dioxide. However, no combustion process is ideal and uncombusted methane and carbon monoxide will be present in the exhaust from the engine. The preferred technique to remove these pollutants from the exhaust, before they are released to the atmosphere, is to use a catalytic converter to facilitate the total combustion of methane to carbon dioxide.

Catalytic converters for vehicles are typically realized as noble metal nanoparticles dispersed on the surface of a high-surface-area metal oxide such as alumina (Al_2O_3), or ceria (CeO_2). The catalyst material is coated on the inside of a ceramic or metallic substrate, that features many small channels through which the exhaust flows. The pollutants in the exhaust adsorb to the surface of the metal nanoparticles where they decompose and transform into less harmful products which are released to the atmosphere. Since the metal nanoparticles are small, the total surface area of the metallic phase is huge even for a small total amount of metal. The metal oxide support material keeps the metal particles well dispersed and prevent them from sintering together. For methane oxidation, palladium is the metal that gives the highest catalytic activity during oxygen excess [5], and investigations of palladium catalysts for methane oxidation have been the main focus of this work, primarily using X-ray absorption fine structure (XAFS).

Unravelling the catalyst structure-activity relationship

The traditional goal of catalyst design is to produce a catalyst that maximizes the catalytic activity. That is, for the reaction conditions of interest the conversion rate of reactant molecules should be as high as possible for a given amount of catalyst. In order to develop improved catalyst formulations, it would be highly beneficial to have a good understanding of the chemical and physical phenomena that are responsible for the catalytic reaction. Both the chemical composition and the atomic-scale physical structure of the catalyst are important in this respect. Real-world catalysts are, however, typically multi-component systems with a heterogeneous structure that makes detailed studies of the interaction between the catalyst and gas phase molecules difficult. Furthermore, the chemical and physical structure of the catalyst is not static and could change depending on the operating conditions of the catalyst. Many different approaches, both theoretical and experimental, have been developed in catalysis research to investigate the connection between catalytic activity and the physical and chemical structure of a catalyst, and it is likely that the combination of several techniques will be required to obtain a more complete picture.

One approach to study fundamental aspects of a catalytic reaction, is to investigate adsorption and reaction on clean, well defined, metal surfaces. These types of clean surfaces can typically only be obtained under ultra-high vacuum conditions, and a number of experimental techniques have been developed to analyze surfaces under these conditions. This type of research on metal surfaces, and other types of surfaces and interfaces, is often referred to as surface science. Many important fundamental aspects of catalytic reactions have been learned from surface science experiments, which has been recognized, for example, by the awarding of 2007 Nobel Prize in chemistry to Gerhard Ertl, for his studies on iron catalysts for the Haber-Bosch process and carbon monoxide oxidation over Pt surfaces [6]. However, the clean surfaces studied with surface science techniques and the ultra-high vacuum conditions are quite different from real-life catalysts, where most catalysts are operated at a pressure close to atmospheric. In catalysis research the terms *materials gap* and *pressure gap* are often used to indicate the difference in materials and pressure between surface science experiments and catalyst applications [7, 8].

A different approach to study catalytic reactions is to use a catalyst with a realistic

structure, and test the catalytic activity and selectivity in a reactor that mimics the real-life operating conditions, together with simultaneous in situ characterization by some spectroscopic technique. This approach is called operando spectroscopy [9], and can be used together with different spectroscopic techniques such as IR spectroscopy, UV-vis spectroscopy, X-ray absorption fine structure, and also X-ray diffraction. Using operando spectroscopy, the relationship between the structure and composition of the catalyst, and the catalytic activity can be studied directly, since the state of the catalyst is probed using spectroscopy simultaneous to the collection of kinetic data.

Objectives

In this thesis, the total oxidation of methane over palladium catalysts has been investigated using operando X-ray absorption fine structure, with the primary aim to study the active phase of palladium during the catalytic reaction. The catalysts studied have been palladium model catalysts prepared by incipient wetness impregnation. These catalysts have complex heterogeneous structure, similar to realistic catalysts, but contain fewer components in order to focus the investigations on the effects of the individual components. A particular focus of the experimental work has been placed on data processing, in order to extract more information from the collected data sets. For example, the use of phase sensitive detection to acquire more noise free data-sets, and complementary theoretical studies have also been performed in order to explore how different structures effect the X-ray absorption spectra. A further objective has been to investigate different support materials, as well as how modifications of the Pd metal phase effect the catalytic activity.

Chapter 2

Operando Spectroscopy

Time is a parameter of high importance in the study of a catalytic reactions. The activity of a catalyst refers to the amount of reaction product formed as a function of time, with typical catalysts having a turnover frequency of 10^{-2} to 10^3 s^{-1} . This means that ideally we should be able to measure changes in the catalyst chemistry and structure on a timescale from minutes to milliseconds [10]. The term *operando spectroscopy* has been established in catalysis research to describe an experiment with *simultaneous* activity measurements and spectroscopic characterization of a catalyst.

In situ characterization

In situ characterization or in situ spectroscopy, refers to spectroscopic measurements of a catalyst under some specific conditions of temperature, pressure, concentration, or other important experimental parameters. Operando spectroscopy can be viewed as a type of in situ spectroscopy where spectra are recorded in situ under reaction conditions with simultaneous activity measurements. Other types of in situ spectroscopy experiments are possible, for example recording spectra during different pre-treatment conditions, or temperature programmed oxidation/reduction.

Spectroscopic Techniques

Operando spectroscopy can be performed using several different spectroscopic techniques. Each spectroscopic technique has its own sensitivity and limitations, which means that one single spectroscopic technique will not provide all the necessary physical and chemical information (*e.g.* oxidation state, coordination environment, metal dispersion) [11]. The work in this thesis is centered around the use of X-ray absorption spectroscopy for operando spectroscopy studies. X-ray absorption spectroscopy has become a widely used technique in catalysis research to characterize the catalyst composition and identify the active phase of the catalyst and more details on X-ray absorption spectroscopy are given in the following chapters. Other spectroscopic techniques used for operando experiments include infrared (IR) spectroscopy, Raman spectroscopy, UV-Vis spectroscopy, ambient-pressure

X-ray photoelectron spectroscopy (XPS), electron paramagnetic resonance (EPR), and also X-ray diffraction (XRD). The choice of experimental technique is dependent upon several factors, the main limiting factor being that the technique must be compatible with the type of sample, environment, and reaction cell. Moreover, the technique must be able to provide relevant information on the investigated catalyst. Most spectroscopic techniques for in situ characterization are based on a photon-in-photon-out principle where the sample is stimulated with electromagnetic radiation and the response is measured by detecting electromagnetic radiation, see Figure 2.1 for an illustration. This approach is used since photons are able to escape from the sample and be detected also when gas phase molecules are present around the sample. Capturing heavier particles, such as electrons diffracted or emitted from the catalyst, under these conditions is typically difficult as the mean free path for these particles will be short unless the sample is held under ultra-high vacuum conditions, although techniques such as ambient pressure XPS have been developed which can to a certain extent overcome this limitation.

Infrared spectroscopy has a long history in the investigation of catalytic reactions. The earliest operando spectroscopy paper was possibly published in 1977 by Okawa, Onashi, and Tamaru [12], describing experiments where pulses of reactants were fed to an infrared cell containing a catalyst while simultaneously performing a chromatographic analysis of the reaction products [9, 12]. The typical use of infrared spectroscopy is to identify adsorbed species on the catalyst since the absorption bands of vibrationally active molecules are changed by the adsorption process. There is a range of infrared spectroscopy techniques suitable for catalysis experiments. For powder catalysts, the three most common techniques used are transmission-absorption IR spectroscopy, diffuse reflectance infrared Fourier transform spectroscopy (DRIFTS), and attenuated total reflection IR spectroscopy. In this thesis, operando DRIFTS and mass spectrometry were used in **Paper V** to study methane oxidation over bimetallic Pd–Pt catalysts. DRIFTS has become a widely used spectroscopic technique in catalysis as powder catalysts can be analyzed under in situ conditions with a limited amount of sample preparation. For the traditional transmission-absorption measurement, the sample must be prepared as a self-supporting pellet with a suitable IR transparency, DRIFTS can instead be used directly on powder samples, which can avoid diffusion limitations in tightly pressed samples, and there is also no requirement for IR transparency [13]. The major downside with the DRIFTS technique is that there is no linear relation between the intensity of the absorption band and the concentration of the absorbing species, which makes quantitative analysis complicated. In operando spectroscopy, the main focus is usually on the dynamics of the catalyst material during reaction conditions, and how the adsorbed species and surface structure change in relation to the catalytic activity, so spectroscopic quantification is usually not a first priority. The identity of surface species can be an important piece of information to understand the mechanism a catalytic reaction, therefore, the combination of infrared spectroscopy with online kinetic measurements has been a widely used approach for operando catalysis studies.

Raman spectroscopy is another spectroscopic technique that has been frequently used for operando studies of catalysts. Although not having the inherent surface sensitivity often found with infrared spectroscopy, the different selection rules between Raman and IR can make Raman spectroscopy the preferred choice for some catalyst systems. In particular,

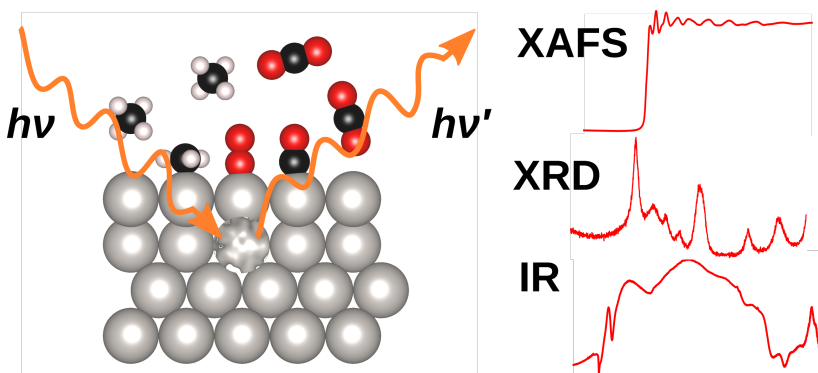


Figure 2.1: Cartoon illustrating an in situ spectroscopy experiment with a photon-in-photon-out measurement technique, the photons are able to probe the catalytic material also with gas phase molecules present. This is the basis for techniques such as XAFS, XRD, and IR spectroscopy.

supported metal oxide catalysts are often found to have properties advantageous for in situ Raman studies [9]. UV-Vis spectroscopy can also be used for operando studies of catalysts, however, due to the difficulties of preparing transparent films of solid catalysts, spectra must almost always be collected in a diffuse reflectance geometry. While UV-Vis spectroscopy directly probes the electronic structure the resulting spectra are often complex containing many broad overlapping bands, making interpretation of the spectra more difficult [11]. Although not strictly a spectroscopic technique, powder X-ray diffraction is a catalyst characterization technique that works well for in situ experiments. Due to the penetrating power of hard X-rays compared to light in the UV-Vis-IR wavelength region, X-ray diffraction can be relatively easily adapted for in situ experiments with control over heating and gas phase environment around the sample. The obvious drawback of this technique is that diffraction requires crystalline materials, and for supported metal catalysts, X-ray diffraction will not be sensitive to metal nanoparticles smaller than 2-3 nm [14].

In recent years, advancements have been made in methods that have primarily been used under ultra-high vacuum conditions, in order to make measurements also under higher pressures. X-ray photoelectron spectroscopy (XPS) has been a widely used technique for studying chemical reactions on solid surfaces due to its high surface sensitivity and element specificity. XPS has traditionally been an ultra-high vacuum technique since it is dependent on capturing photoelectrons emitted from surface atoms, but ambient-pressure XPS instruments have been constructed for many years and are continuously improved [15]. The basic design of these instruments consists of a sample enclosed by an elevated pressure volume, and an X-ray source and an electron energy analyzer kept at ultra-high vacuum conditions. The X-rays enter the elevated pressure volume via an X-ray transparent window or multiple stages of differential pumping. The photoelectrons are collected through a small aperture in the elevated pressure volume close to the sample, which leads to a differentially pumped electron energy analyzer. Using this type of setup,

experiments were performed at pressures up to about 1 mbar [15]. The main factor limiting experiments at higher pressures is the attenuation of photo electrons due to scattering by gas phase molecules [15]. This technique has been improved by using synchrotron light sources, which provide much more intense X-rays and a higher flux of photoelectrons. A second improvement is the use of electrostatic lenses in the differential pumping stages in the energy analyzer, which refocus the electrons onto the apertures separating the stages. Incorporating these improvements, modern synchrotron-based ambient pressure XPS can be used at pressures above 7 mbar [16, 17]. In situ methods have also been developed for transmission electron spectroscopy, often referred to as environmental TEM. Similar to XPS, the electrons used to image the sample are scattered by gas phase molecules, so the volume with higher pressure around the sample should be small, while the rest of the microscope column should be kept under high vacuum. This is accomplished using apertures and differential pumping, so that the volume with increased pressure is only in the immediate vicinity of the sample. Using this approach, it is possible to obtain atomic resolution images using pressures up to a few millibar [18, 19].

Time resolution

For operando spectroscopy, the spectroscopic technique must have a sufficiently high time resolution to capture changes in the catalytic material that occur during reaction conditions. As mentioned above, the kinetics of a catalytic reaction can change on time scales on the order of minutes to milliseconds, so depending on the experiment, the spectroscopic technique used in an operando experiment must typically achieve a time-resolution in this range. There is often a trade-off between obtaining high time resolution and recording high-quality spectra, which is an important parameter in the design of operando experiment. The acquisition time must be long enough to obtain acceptable levels of random noise, but in order to obtain significantly higher time resolutions, it might be necessary to change to a different mode of acquisition. For XAFS, a good example of this is energy-dispersive XAFS that can provide time resolution in the millisecond range, which is much higher than what traditional monochromator based beamlines can achieve (see section 3.1 for more details). However, the energy-dispersive XAFS technique usually results in less detailed spectra due to the lower energy resolution and higher sensitivity to beam instabilities.

Transient kinetic measurements

Kinetic data from a catalyst is often recorded under steady state conditions (*i.e.* no variations in temperature, pressure, and reaction rate), however, to obtain detailed understanding of the reaction mechanism, it is often necessary to do experiments in a non-steady-state or transient regime. In catalysis, chemical transient kinetics refers to the analysis of kinetic data starting from a perturbation of one of the parameters controlling the kinetics of the catalytic reaction, until a steady state has been reached. The two main transient kinetic methods are to either vary the chemical composition of the feed gas, such as rapidly changing the concentration of one of the reactants, or to change the

isotopic composition of the feed gas without changing the chemical composition [20]. In principle, it would also be possible to perform transient kinetic measurements by changing the temperature, but in practice it is difficult to change the temperature of the system quickly enough compared to the changes in the kinetics when a catalytic reaction adapts to this perturbation.

One method for transient kinetic experiments using changes to the isotopic composition is SSITKA (steady-state isotopic transient kinetic analysis), originally developed by Happel, Bennet, and Biloen [21–23]. This method has, for example, been used to study methane oxidation over Pd/Al₂O₃ [24]. Here, transient kinetics were observed by switching ¹⁶O₂ to ¹⁸O₂ while flowing methane over the catalysts, and oxygen containing species in the outlet such as ¹⁶O₂, ¹⁸O₂, ¹⁶O¹⁸O, C¹⁶O₂, C¹⁸O₂, and C¹⁶O¹⁸O were monitored by mass spectrometry. Notably, C¹⁶O₂ was detected in the outlet up to eight minutes after the feed had been switched from ¹⁶O₂ to ¹⁸O₂, showing that oxygen from the PdO lattice must be taking part in the methane oxidation reaction in a Mars-van Krevelen redox mechanism.

In this thesis, we have performed transient kinetic measurements mainly through pulse-response experiments, where the concentration of one or several reactants are changed periodically between two values. The rapidly changing inlet concentrations can induce changes in the surface coverage of reactants on the catalyst, or reconstructions of the catalyst surface. By observing the effect on the catalytic conversion and the effect on the catalytic material by in situ spectroscopy, insight on the catalytic mechanism can be obtained which would not be available from steady-state experiments. Periodic pulses of reactants can in certain cases also be used to increase the catalytic activity compared to steady-state conditions. At low temperature, the oxidation of CO over platinum catalysts is limited by the strong adsorption of CO to the platinum surface compared to oxygen, which prevents oxygen from adsorbing and dissociating on the catalyst surface. By introducing periodic pulses of oxygen, the oxygen coverage on the surface was increased, giving an increased conversion for every subsequent oxygen pulse [25]. In some catalyst applications, there is also a variation in the feed gas composition over time, and periodic pulsing can be a method to achieve similar changes in a controlled manner. For example, in automotive catalysis the composition of the exhaust changes depending on how the vehicle is operated.

An extension of the pulse-response technique for operando spectroscopy is modulation excitation spectroscopy. In this technique, one experimental parameter such as concentration, temperature or pressure is varied periodically (modulated) while simultaneously collecting spectroscopic data. The main requirement for using this technique is that the catalyst (and thus the spectroscopic data) changes periodically and reversibly with time, as a function of the periodic modulation. The main benefit of modulation excitation spectroscopy is the increased sensitivity in the spectroscopic data to small changes in the catalyst material, similar to how small signals can be extracted using a lock-in amplifier. Section 3.4 explains in more detail how modulation excitation spectroscopy can be used together with X-ray absorption fine structure for experiments in catalysis.

Chapter 3

X-ray absorption fine structure

X-ray absorption fine structure (XAFS) is a type of absorption spectroscopy using X-rays. The technique is similar to other types of absorption spectroscopy involving lower energy radiation, and is also called X-ray absorption spectroscopy (XAS). X-ray absorption fine structure requires a broadband, tunable, source of X-rays, which means that measurements are primarily performed using synchrotron light sources.

X-ray absorption spectra

The basic setup used for recording a *transmission mode* X-ray absorption spectrum is shown in Figure 3.1. The intensity of the X-rays are recorded before and after being transmitted through the sample, and by using a monochromator to measure the intensities at different energies the absorption spectrum can be constructed using the Lambert-Beer law

$$\mu x = \ln \frac{I_0}{I_t} \quad (3.1)$$

where μ is the linear absorption coefficient, x is the thickness of the sample, I_0 is the incident intensity, and I_t is the transmitted intensity. The XAFS spectrum is measured at an absorption edge which is a sharp increase in absorption due to the excitation of core electrons out of their bound states and into the continuum, creating photo-electrons. Figure 3.2 shows a spectrum of a Pd foil recorded in transmission mode, the absorption edge is close to 24 350 eV and is due to the excitation of 1s electrons which is also called a K edge spectrum.

The structural information in the XAFS spectrum is found in the small variations, or fine structure, in the absorption coefficient near the absorption edge and at higher energies. For analysis the XAFS spectrum is typically subdivided into two regions. The region near the absorption edge which is called *X-ray absorption near edge structure* (XANES), and the region at energies higher than the absorption edge is called *extended X-ray absorption fine structure* (EXAFS).

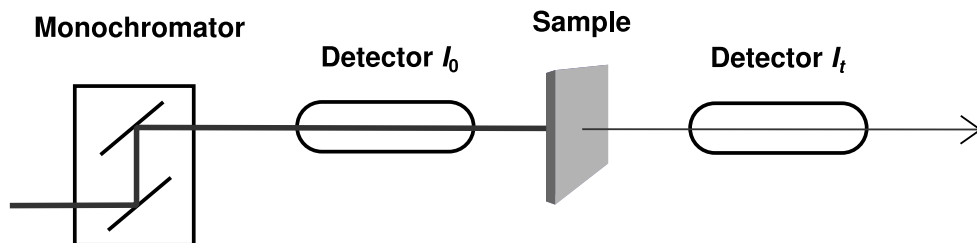


Figure 3.1: Schematic illustration of a transmission mode X-ray absorption fine structure experimental setup.

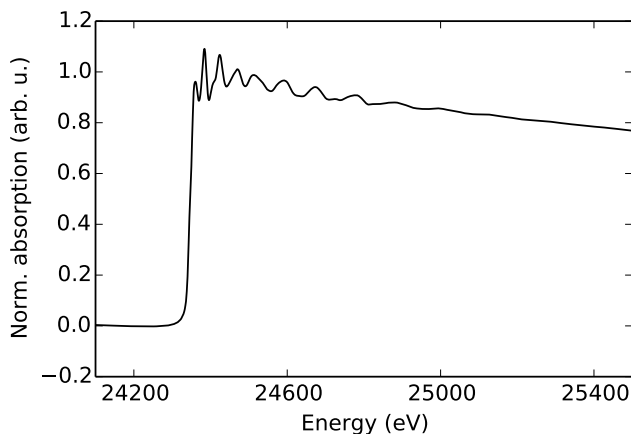


Figure 3.2: XAFS spectrum of a palladium foil recorded in transmission mode.

The shape of the XANES is influenced by the presence of high-lying unoccupied bound states that can accept the excited core electrons. The most straightforward approach to analysis of XANES is fingerprinting, which means directly comparing the measured spectrum to the spectrum of a known compound or a simulated spectrum from a calculation. XAFS spectra can be calculated from first principles with high accuracy. Such calculations were performed in **Paper VI** to investigate the effect of particle size, morphology, and oxidation state on the Pd K edge XAFS spectra. Fingerprinting can be improved by using modulation excitation spectroscopy, as described in Section 3.4, since small changes in the XAFS spectra can be isolated. The fine structure in the EXAFS region is due to backscattering of the photoelectron, which is created in the excitation, from nearby atoms that modulate the absorption coefficient. The EXAFS region can be analyzed to determine the structure around the absorbing atom, as described in Section 3.2.

Recording an XAFS spectrum with a step-scan monochromator typically takes many

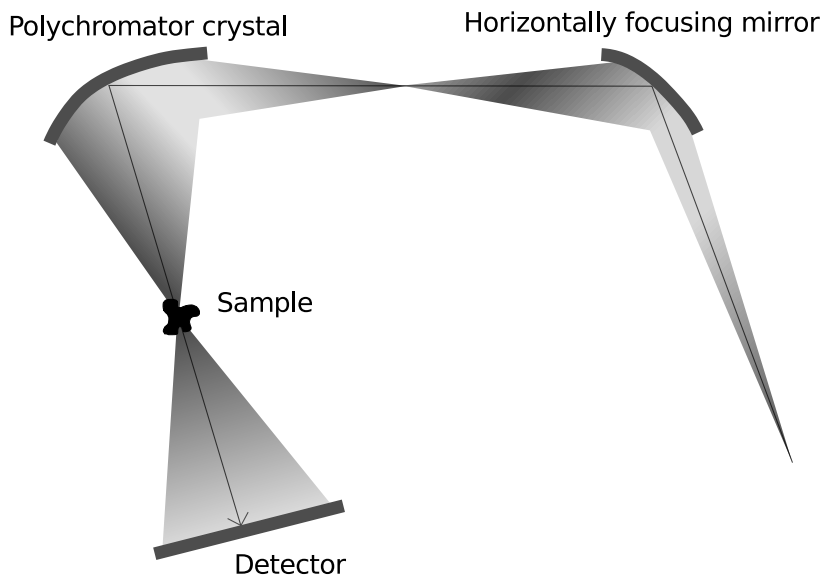


Figure 3.3: Setup of an energy-dispersive XAFS beamline. The horizontally focusing mirror increases the divergence of the beam before the polychromator crystal, which disperses the X-rays and focus them through the sample. The beam that diverges from the sample hits a position sensitive detector.

minutes, however, for in situ studies of catalytic reactions it would many times be beneficial to record spectra with higher time resolution. Two techniques that can achieve this are quick XAFS and energy-dispersive XAFS. In quick XAFS a faster scanning monochromator is used that moves continuously through the energy range of interest, so that it is possible to acquire a full spectrum in less than 1 s [26]. Energy-dispersive XAFS uses a distinctly different setup where the monochromator is replaced by a polychromator crystal that disperses the X-rays into its different frequencies and focus them through the sample [27]. The beam that diverges on the other side is incident on a position sensitive detector where the high energies are recorded at one end and the low energies at the other end, this type of setup is shown in Figure 3.3. The time-resolution is only limited by the time it takes to read out the detector and the acquisition time can be on the order of tens of milliseconds. There are drawbacks with this method that can result in reduced spectral quality such as decreased energy resolution and problems correcting for beam instabilities since I and I_0 cannot be measured simultaneously. The majority of the XAFS experiments in this thesis were performed with the energy dispersive XAFS technique. The model catalysts used in our studies have a heterogeneous structure, and due to this we have accepted the trade-off in spatial resolution for a higher time resolution. The main objective in our studies has been to study the dynamics in the catalyst structure during changing operating conditions, rather than an exact characterization of the catalyst structure under constant reaction conditions.

EXAFS analysis

The photoelectron that leaves the atom due to the absorption of X-rays will have both particle and wave characteristics. The outgoing photoelectron wave can be scattered back from neighbouring atoms to the absorbing atom, which leads to interference between the outgoing, and the backscattered photoelectron. As a result of this, the absorption coefficient is modulated so that it is enhanced at energies where constructive interference occurs [13]. The oscillations increase in intensity with increasing number of neighbouring atoms, and the frequency depends inversely on the interatomic distances. Mathematically this is described by the EXAFS equation [13]

$$\chi(k) = \sum_j A_j(k) \sin[2kr_j + \phi_j(k)] \quad (3.2)$$

where $\chi(k)$ is the EXAFS function, j is the label of the coordination shells around the absorbing atom, $A_j(k)$ is the amplitude due to the scattering intensity from the j^{th} shell, r_j is the distance between the absorbing atom and the atoms in the j^{th} coordination shell, and $\phi(k)$ is the total phase shift. The wavenumber k is related to the photoelectron kinetic energy through $k = \frac{2\pi}{h} \sqrt{2m_e E_k}$, where m_e is the electron mass and E_k the kinetic energy of the photoelectron. Each coordination shell contributes with a sine function multiplied by an amplitude, and this amplitude is proportional to the number of atoms in the coordination shell N_j [13]:

$$A_j(k) = N_j \frac{e^{-2r_j/\lambda(k)}}{kr_j^2} S_0^2(k) F_j(k) e^{-2k^2\sigma_j^2} \quad (3.3)$$

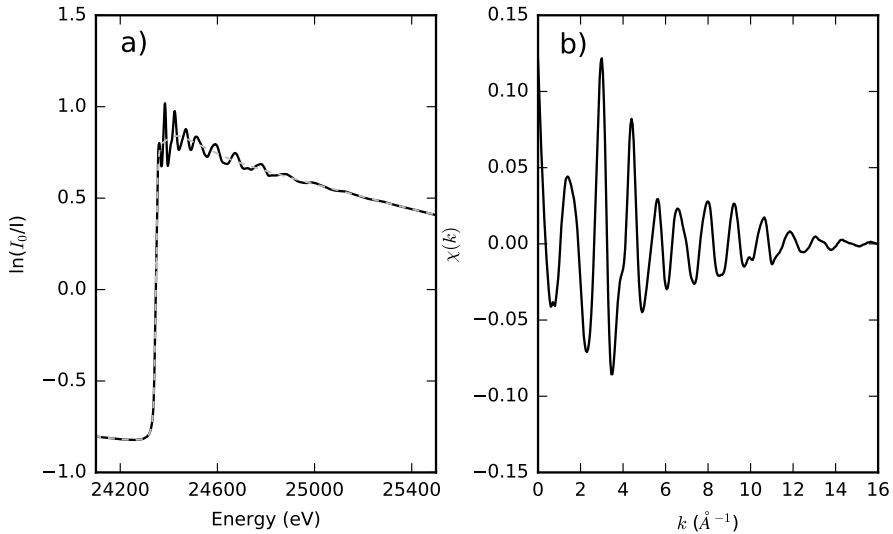


Figure 3.4: (a) XAFS spectrum of a palladium foil (solid) with fitted background curve (dashed). (b) EXAFS function obtained by subtracting the background function from the measured spectrum.

Other terms included are the exponential attenuation of electrons propagating through the material ($e^{-2r_j/\lambda(k)}$), a correction for relaxation effects in the absorbing atom (S_0), the effect of lattice vibrations ($e^{-2k^2\sigma_j^2}$), and $F_j(k)$ which is the effective scattering amplitude.

EXAFS is often analyzed by extracting $\chi(k)$ from the experimental data, and then performing a curve fit to a theoretical scattering path. The experimental $\chi(k)$ is extracted by subtracting a smooth background function that is fitted to the measured spectrum, as shown in Figure 3.4. A theoretical scattering path is constructed by considering a model structure that should be close to the material that has been measured. A numerical calculation is performed that estimates the unknown functions in the EXAFS equation like $F_j(k)$, $\phi_j(k)$, and $e^{-2r_j/\lambda(k)}$ based on the model structure. The EXAFS equation is set up for the model structure and the difference to the experimental EXAFS function is minimized by varying parameters of interest like the interatomic distance r_j and coordination number N_j . By this approach, the best-fit parameters for variables in the EXAFS function such as r_j and N_j can be determined.

The different coordination shells that contribute to the EXAFS function can also be visualized by Fourier transformation, which will separate the different sine waves that contribute to the EXAFS function. The magnitude of the Fourier transform will show a curve similar to a radial distribution function, Figure 3.5 shows the Fourier transform of an EXAFS function from a palladium foil. The peaks correspond to the different coordination shells in the Pd face centred cubic structure, however, the positions on the R axis do not exactly correspond to the interatomic distances since the phase shift ($\phi(k)$) is not taken into account.

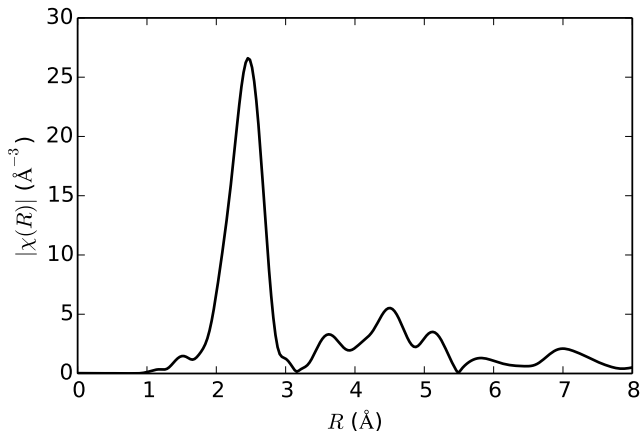


Figure 3.5: Fourier transformed EXAFS function from a palladium foil.

Multiple-scattering XAFS calculations

Theoretical scattering paths for EXAFS fitting as well as simulated XANES spectra were calculated with the FEFF real-space multiple-scattering code [28]. FEFF is a first-principles code where the main input is the atomic coordinates and the type of atoms in the system. One atom is designated as the atom where the excitation occurs and the orbital of the electron that is excited to create the photoelectron is selected. Scattering of the photoelectron from atoms far away from the absorbing atom is not significant for XAFS, so for extended materials, a cluster with a representative geometry can be cut out and the absorbing atom placed in the centre; periodic boundary conditions are not used by FEFF.

XAFS can be described, in the single electron and dipole approximation, as the dipole mediated transition of a deep core electron $|i\rangle$ into some unoccupied state $|f\rangle$. The probability for this transition is described by Fermi's Golden Rule [29]

$$\mu(E) \propto \sum_f |\langle f | \hat{\epsilon} \cdot \mathbf{r} | i \rangle|^2 \delta(E - E_f) \quad (3.4)$$

where $\hat{\epsilon}$ is the X-ray polarization vector, $|i\rangle$ is an initial core state, and $|f\rangle$ is a final state. The sum over final states and the energy-conserving delta function can be compactly written in terms of the Green's operator $G(E) = 1/(E - H - i\zeta)$, where ζ denotes the net lifetime, including effects of extrinsic and intrinsic losses [30]. Using the spectral representation $\sum_f |f\rangle \delta(E - E_f) \langle f| = (-1/\pi) \text{Im} G(E)$, we can rewrite Eq. (3.4) [31]

$$\mu(E) \propto -\frac{1}{\pi} \text{Im} \langle i | \hat{\epsilon} \cdot \mathbf{r} G(E) \hat{\epsilon} \cdot \mathbf{r} | i \rangle \quad (3.5)$$

In the position representation, G can be written in terms of the single-particle wavefunc-

tions ψ_n of energy E_n

$$G(\mathbf{r}, \mathbf{r}'; E) = \sum_f \frac{\psi_n(\mathbf{r})\psi_n^*(\mathbf{r}')}{E - E_n + i\zeta} \quad (3.6)$$

The wavefunctions ψ_n are solutions to the equation

$$h'\psi_n = \left(\frac{p^2}{2m} + V'_{\text{coul}} + \Sigma(E) \right) \psi_n = E\psi_n \quad (3.7)$$

where V'_{coul} is the net Coulomb potential felt by the photoelectron and $\Sigma(E)$ is the self energy, which is analogous to the exchange-correlation potential V_{xc} in ground-state calculations [30, 31].

The Green's function separates the contributions from the central atom and multiple scattering contributions from the neighbouring atoms, so that we can write [30]

$$G(\mathbf{r}, \mathbf{r}'; E) = G^c(\mathbf{r}, \mathbf{r}'; E) + G^{\text{SC}}(\mathbf{r}, \mathbf{r}'; E) \quad (3.8)$$

The scattering portion of the Green's function G^{SC} can be calculated from [31]

$$G^{\text{SC}} = (1 - G^0 T)^{-1} G^0 \quad (3.9)$$

where G^0 is the free electron propagator and T is the scattering operator. This part can be efficiently calculated by expansion into a series

$$G = G_0 + G_0 T G_0 + G_0 T G_0 T G_0 \quad (3.10)$$

Each term in the expansion describes an order of scattering. $G_0 T G_0$ describes all possible ways that the photoelectron can scatter by only one neighbouring atom. $G_0 T G_0 T G_0$ describes all the ways that a photoelectron can scatter from two surrounding atoms. The next term in the series describes all the ways that a photoelectron can scatter three times, and so on [32]. This means that the multiple scattering contribution to the absorption coefficient can be expanded as a sum of terms, each which corresponds to a scattering path that begins and ends at the central atom, which involves scattering one or more time from atoms in the vicinity [31].

Calculating multiple scattering using the series expansion above typically works well for the EXAFS region, however, for the region close to the absorption edge, the XANES region, this type of calculation may not be accurate. Here it is more reliable to calculate G^{SC} through matrix inversion according to Equation 3.9. This will include the contributions from all orders of scattering, however, this is much more computationally expensive. In FEFF this type of calculation is called *full multiple scattering* and was used to calculate the simulated XANES spectra in **Paper VI**. The theoretical standards used for EXAFS fitting in **Paper I and II** were calculated using the series expansion approach, which is called *path expansion* in FEFF.

Modulation excitation spectroscopy

Modulation excitation spectroscopy is an experiment where at least one experimental parameter is periodically varied while simultaneously collecting spectroscopic data [33].

Examples of experimental parameters that can be varied are concentration, temperature, pressure, potential, or magnetic field. This method is not limited to any particular spectroscopic technique, it has been used together with IR spectroscopy [33], X-ray diffraction [34], Raman spectroscopy [35] and X-ray absorption fine structure [36, 37]. In **Paper I and II** modulation excitation spectroscopy was used together with X-ray absorption fine structure in rich-lean cycling experiments. The main advantage of using the modulation excitation approach is that the resulting spectra can be analysed using the phase sensitive detection technique, which is described by the equation [38]

$$A_k^{\phi^{PSD}}(E) = \frac{2}{\tau} \int_0^{\tau} A(E, t) \sin(k\omega t + \phi_k^{PSD}) dt \quad (3.11)$$

where $A(E, t)$ is the original signal (i.e., the XAFS spectra) as a function of time t and energy E , k determines the frequency of the demodulation ($k = 1$ is the fundamental harmonic), ω is the frequency of the periodic modulation, ϕ_k^{PSD} is the demodulation phase angle, and τ is the modulation period. $A_k^{\phi^{PSD}}(E)$ are the phase resolved or demodulated spectra that result from the transformation from the time domain to the phase angle domain by Equation 3.11 for phase angles between 0 and 360°. The value in the modulation excitation technique lies in the advantageous properties of the demodulated spectra [37]:

- They contain only the contribution from species that respond to the external stimulation with the same frequency. This gives a significant increase in sensitivity to active species that respond to the stimulation, compared to static signals produced by spectator species.
- The signal-to-noise ratio is improved because noise has a different frequency compared to the periodic perturbation and will be filtered in the demodulated spectra.
- If multiple intermediate species occur with a phase delay (e.g, oxidation and reduction via multiple oxidation states) they can in principle be differentiated.

One of the major limitations of using XAFS to study catalysts is the lack of surface sensitivity. Since catalysis is a surface phenomenon it would be advantageous to selectively probe the surface of the metal nanoparticles, however, in XAFS there will always be a contribution from the bulk of the nanoparticles. The use of the modulation excitation approach can be one way to work around this limitation, since the static signal from the bulk atoms can be filtered [37].

Example of demodulated XAFS spectra are shown in Figure 3.6 where a flow of 1.5% oxygen was switched on and off over a Pd/Al₂O₃ catalyst every three minutes while flowing a constant concentration of 0.1% methane. The demodulated spectra isolate the changes in the spectra due to the periodic modulation, and is a type of difference spectrum. Here, we see the demodulated spectra from oxidation and reduction of Pd; the demodulated spectra are very similar to the difference spectrum of metallic Pd and PdO shown in Figure 3.6. In **Paper I**, modulation excitation spectroscopy was used for fingerprinting similar to the example above. In **Paper II**, a fitting model was used to obtain quantitative data from the demodulated spectra on the oxidation state of Pd during methane oxidation.

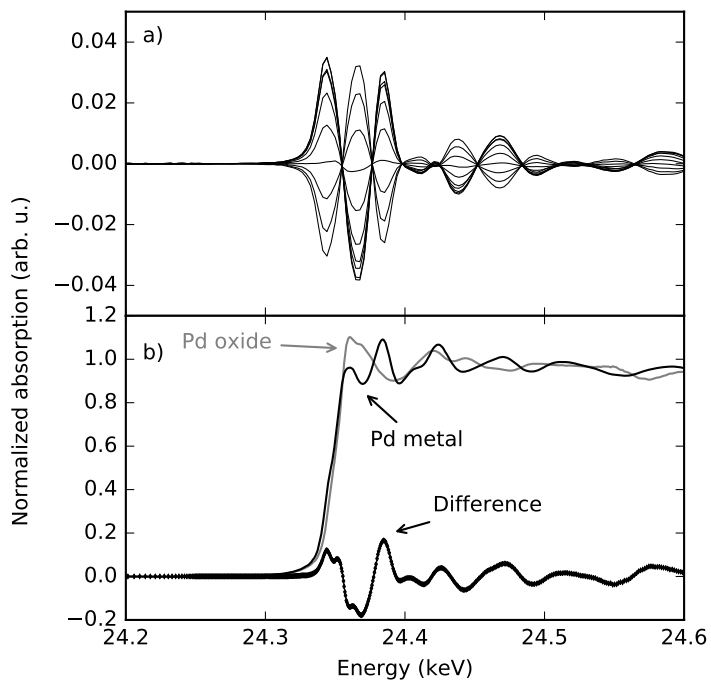


Figure 3.6: (a) Demodulated XAFS spectra from Pd/Al₂O₃ where a flow of 1.5% oxygen was switched on and off every three minutes while flowing a constant concentration of 0.1% methane at 360 °C. (b) Spectra of palladium metal, palladium oxide, and the difference spectrum of Pd and PdO.

Chapter 4

Model catalysts in catalysis research

Catalysts used in real-life applications are typically complex multi-phase systems. Supported metal catalysts can consist of several different active metals deposited on a support material that is a mix of several different metal oxides. The exact formulation of these catalysts has in many cases developed over a long time where components have been added and removed in a more or less trial-and-error fashion. In order to study more fundamental aspects of catalysis, researchers have often used simplified model catalysts that are easier to characterize. However, this also introduces the problem of whether the results obtained on these model catalysts also translate to more complex catalysts.

Scaling back complexity from realistic catalysts

An automotive three-way catalyst is a good example of a supported metal catalyst with a complex structure. The noble metals platinum, palladium, and rhodium are typically included as active components in these catalysts. Platinum and palladium have been known for a long time to be very active for the oxidation of carbon monoxide and hydrocarbons, and by combining them with rhodium, also good activity for the reduction of NO_x can be achieved [39]. Alternative approaches, such as Pd-only three-way catalysts have also been demonstrated [40]. The support material is a mix of several metal oxides providing different functions. A major component of the support material is typically $\gamma\text{-Al}_2\text{O}_3$, which provides a high surface area for the deposited metal nanoparticles as well as a high hydrothermal stability. Another important component is the $\text{CeO}_2\text{-ZrO}_2$ oxygen storage material, which is a reducible material that can store oxygen when excess oxygen is present in the exhaust, and release oxygen when the exhaust is fuel rich [41]. This is an important function in an automotive catalyst since the air-to-fuel ratio varies rapidly during operation of the vehicle, and oxygen storage and release by the catalyst is crucial to maintain high conversion under these conditions. Other metal oxides such as La_2O_3 , Y_2O_3 , Ga_2O_3 can be added as promoters to further improve the oxygen storage

capability [42].

Model catalysts are simplified catalysts developed for research. One common motivation for working with a model catalyst is to study a catalytic reaction with some specific analysis technique, that is not compatible with the type of catalysts used in the real-life application. Moreover, model catalysts can be prepared in order to study the effect of just a single component in the catalyst, eliminating other components that might complicate such a study. One of the most well known model catalysts in catalysis research are single crystal metal surfaces. Research on these model systems is strongly connected to the development of surface science techniques from the 1960's and onwards, which enabled detailed studies of chemical reactions on clean solid surfaces under ultra-high vacuum conditions [43]. Although many important insights have been learned from surface science experiments the experimental conditions are quite, dissimilar compared to realistic operating conditions for most catalysts. This has led to the creation of the terms materials gap and pressure gap to describe the dissimilarity of materials and pressure between surface science experiments and catalyst applications [7, 8].

Many different model catalysts have been developed with the motivation to "bridge the materials gap". One example of such model systems are metal nanoparticles deposited on a single-crystal metal oxide surface, such as Pd nanoparticles deposited on a flat MgO surface [44, 45], see Figure 4.1 for illustrations of different types of catalysts. These model catalysts introduce a support material and the metal nanoparticles have a morphology that is closer to that found in supported metal catalysts, while still providing a flat surface that is compatible with many surface science characterization techniques. For the experiments performed in this thesis, we have used supported metal catalysts prepared through incipient wetness impregnation. These catalysts have a heterogeneous structure similar to many real-life catalysts. However, we still refer to these catalysts as model catalysts since we mostly limit these catalysts to a single metal supported on a single metal oxide support, and do not include additional components such as promoters and stabilizers. Most experiments have been performed on Pd/Al₂O₃ catalysts, but also Pd/CeO₂ as well as bi-metallic Pt-Pd/Al₂O₃ have been investigated.

Synthesis and characterization

The catalysts investigated in this thesis were prepared through incipient wetness impregnation. The preparation starts with a support material, such as γ -Al₂O₃, to which an active metal precursor is added. The active metal precursor is typically an aqueous solution of a metal salt, for a supported Pd catalyst this could be for example Pd(NH₃)₂ solution. In the incipient wetness method, the volume of liquid added is the same as the pore volume of the amount of support material used, so that the liquid is drawn into the pores by capillary action. The impregnated support material is then dried to remove the liquid phase and enable precipitation of the metal in the pores of the support material. The drying step is important to achieve a good distribution of the metal in the pores of the support material, freeze drying can be used to reduce the metal precursor solution mobility and prevent them from migrating out of the pores of the support material. As a last step the catalysts are typically calcined at an elevated temperature to decompose

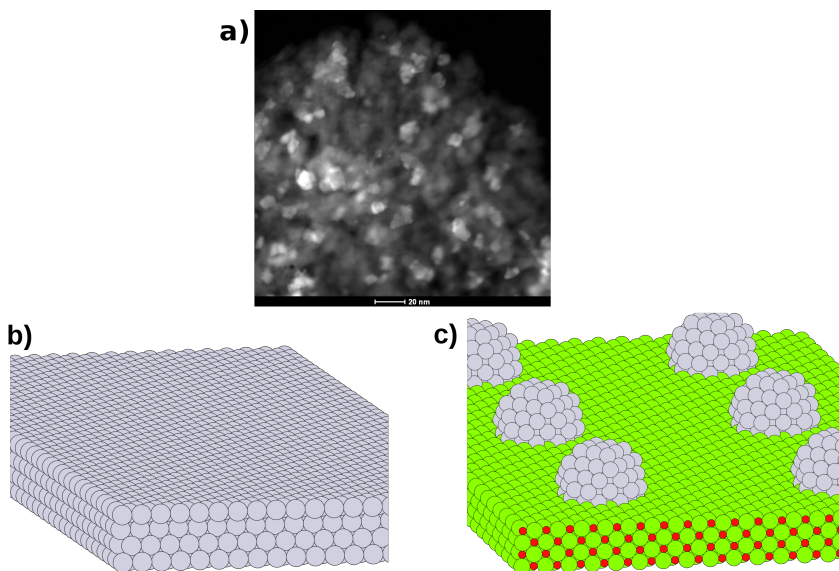


Figure 4.1: (a) TEM image of supported Pd/Al₂O₃ catalyst, the metal nanoparticles are visible as brighter spots in the alumina matrix (b) Illustration of a Pd(111) single crystal surface. (c) Illustration of Pd nanoparticles on top of a flat MgO(100) surface (green=Mg, red=O, and gray=Pd).

and drive off any remaining volatile compounds.

After synthesis the catalyst is often characterized using physio-chemical methods to determine the structure and composition of the prepared catalyst. In this thesis the main characterization methods used were powder X-ray diffraction, chemisorption, and scanning transmission electron microscopy. Several characterization methods are commonly used together as no single technique provides all necessary information, but results that complement each other can be obtained by using multiple characterization techniques.

Powder X-ray diffraction is a commonly used characterization technique in catalysis since catalysts typically contain one or many crystalline phases. The X-ray diffraction pattern is measured by irradiating the sample with monochromatic X-rays and varying the angle between the detector and the X-ray source. At some particular angles, a large increase in intensity will be measured at the detector, due to scattering from different layers in a crystal lattice interfering constructively, which gives a peak in the diffraction pattern. The diffraction pattern can be used to identify the crystalline phases in the sample by comparing the recorded diffraction pattern to diffraction patterns of reference compounds. Furthermore, the widths of peaks in the diffraction pattern contain information about the size of the crystalline domains, since the diffraction peaks will broaden if the crystalline domains are small. For a supported metal catalyst it is typically not possible to obtain a clear diffraction pattern from the metal phase if the metal nanoparticles are smaller than 2-3 nm [14]. Thus, the absence of a diffraction pattern suggests that the metal

nanoparticles are small and well dispersed or form non-crystalline phases. Theoretical models, such as the Scherrer equation, have been developed to calculate the average crystallite size from the peak widths in the diffraction pattern [13].

Chemisorption of gas phase probe molecules can be used to characterize the surface of the catalyst. For supported metal catalysts a probe molecule can be introduced that selectively adsorbs to the metal phase, and by measuring the amount of gas adsorbed the amount of metal exposed (metal dispersion) can be measured. Furthermore, knowing the metal dispersion allows for estimation of the mean particle size, by assuming a specific particle morphology and finding an expression for the volume-to-surface ratio. One major difficulty in dispersion measurements using chemisorption is to determine the correct adsorption stoichiometry, for example CO can adsorb on Pd in a linear mode which gives a CO:Pd ratio of 1:1 but it can also adsorb in bridged modes with CO:Pd ratios of 2:1 and 3:1. Another possible issue is that small probe molecules like hydrogen can dissolve into the bulk of the metal and create phases like palladium hydride, which gives an ill-defined adsorption stoichiometry [46].

Scanning transmission electron microscopy (STEM) is an attractive characterization technique since it gives an image of the catalyst morphology on a length scale close to the atomic level. By imaging supported nanoparticles it is possible to investigate the particle sizes, and particle shapes, and the contact between the particle and support. The particle size distribution can be determined if particle size data is gathered for a large number of particles, provided that the detection probability is the same for all particle sizes. Detection of supported particles can be hampered by poor contrast between the particles and the support, for example if the supported particles are well-dispersed metal oxides.

A further characterization technique, that we utilized in **Paper IV**, is low-energy ion scattering (LEIS). This is a very surface sensitive method that was used to determine the surface composition in the metal phase in our bimetallic Pd–Pt/Al₂O₃ catalysts. The principle behind LEIS is that ions are accelerated to a specific energy and directed toward the surface, the ions collide with surface atoms and are scattered. In this energy range the scattering can be described as hard-sphere elastic scattering [47]. If we consider an ion with mass M_1 and energy $E_0 = \frac{1}{2}M_1v_0^2$ colliding with a surface atom at rest with energy M_2 , then conservation of energy gives

$$\frac{1}{2}M_1v_0^2 = \frac{1}{2}M_1v_1^2 + \frac{1}{2}M_2v_2^2 \quad (4.1)$$

where v_1 and v_2 are the velocities of the scattered ion and target atom, respectively. From this it can be derived that the energy of the scattered ions collected at a specific scattering angle will depend on the mass ratio between the ion and the target atom [47]. For the study in **Paper IV** LEIS was not used to analyze the as-prepared catalysts, but rather the catalysts were pre-treated in hydrogen or oxygen to investigate the effect of oxidation and reduction on the surface composition.

Chapter 5

Methane oxidation over Pd catalysts

Methane is the smallest hydrocarbon and is the principle component of natural gas and biogas. The abundant supplies of natural gas and the clean-burning properties of methane makes methane an attractive fuel, both for generation of electric power and for automotive applications. By using a catalyst, the temperature required to achieve combustion of methane can be drastically lowered, for stationary applications this lower combustion temperature can be used to reduce emissions of NO_x , which is formed from nitrogen in air during high-temperature combustion. For automotive applications, the catalytic combustion of methane is important for exhaust aftertreatment. Methane is a strong greenhouse gas and it is important that emissions of uncombusted methane are minimized. This can be achieved by placing a catalytic converter in the exhaust that facilitates the total oxidation of methane to carbon dioxide and water.

The high symmetry of the methane molecule and the strong C-H bonds make methane the most stable hydrocarbon, and the most difficult to oxidise catalytically. The best performing catalysts today can oxidise methane at a temperature of about 400 °C and higher, however, the expected requirement in the exhaust of a lean burn engine is below 300 °C [48]. The metals palladium and platinum have high activity for methane oxidation and are used as active metals in catalysts for methane oxidation. For platinum the metallic phase is considered to be the most active for methane oxidation, whereas, lean operating conditions can lead to the formation of platinum oxide and deactivation of the catalyst [49, 50]. For palladium the situation is more complex since palladium oxide is the thermodynamically stable phase at temperatures lower than ca 790 °C, which means that palladium oxide can decompose to palladium metal at higher temperatures, or at lower temperatures if the feed gas composition is sufficiently reducing. High activity for methane oxidation in palladium-based catalysts has been attributed to reduced (metallic) palladium [51, 52], metal-supported surface oxide [53], or bulk metal oxide [54, 55]. In single-crystal studies and through computations the PdO(101) facet of palladium oxide has been identified as highly active for methane oxidation, with a low barrier for hydrogen abstraction at under-coordinated surface sites [56, 57]. A detailed microkinetic model has

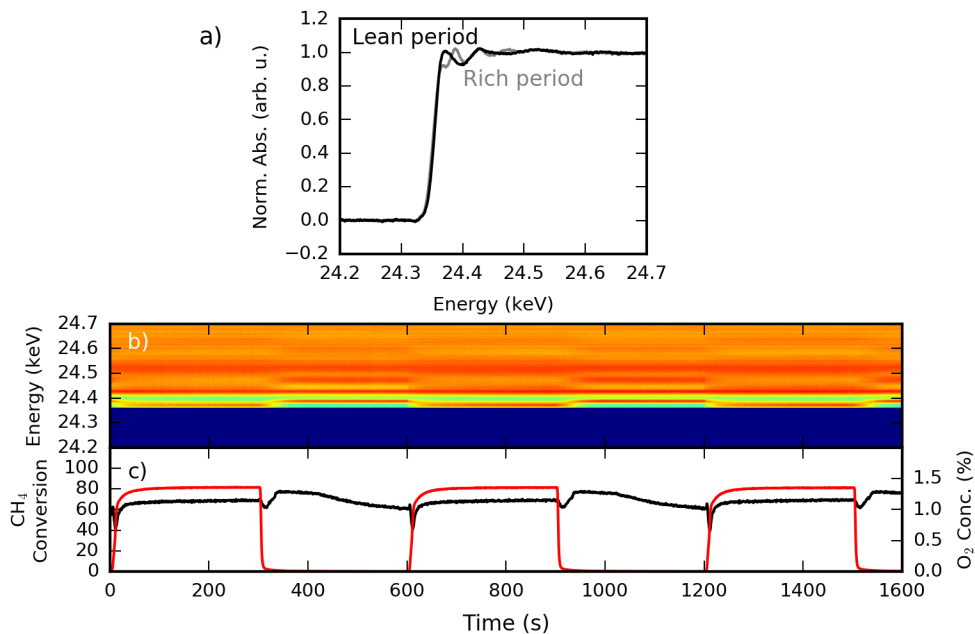


Figure 5.1: Oxidation of 0.1% CH_4 over $\text{Pd}/\text{Al}_2\text{O}_3$ at 350°C , oxygen pulses with a concentration of 1.5% are added to the feed with a duration of 500s. (a) XAFS spectra recorded at the end of the rich and lean periods, (b) color-coded intensities of XAFS spectra (low intensity blue, high intensity red), and (c) methane conversion (black line) and outlet concentration of oxygen (red line).

been developed for methane oxidation over $\text{PdO}(101)$ which is in good agreement with experimental reports [58].

In-situ characterization of palladium catalysts during methane oxidation shows that palladium oxide is the active phase at low temperature and under lean conditions [59, 60]. With a feed gas composition close to the stoichiometric point, palladium was found to be in a mostly reduced state during methane oxidation [61]. It has also been suggested that the equilibrium of bulk-Pd/surface PdO is important for the activity at stoichiometric conditions [62]. Another topic that has been intensely studied in connection to methane oxidation over Pd catalysts is the inhibiting effect of water at low temperatures. Addition of water to the feed has been demonstrated to inhibit methane oxidation over Pd catalysts at temperatures lower than 450°C [63]. Desorption of water was found to be delayed compared to other reaction products at temperatures below 450°C , which indicates that water produced as a reaction product can have an inhibiting effect on methane oxidation over Pd at low temperatures [64].

Oxidation state of Pd during methane oxidation

In order to further investigate the structure-activity relationship of methane oxidation over Pd catalysts we performed an operando study with time-resolved XAFS spectroscopy (**Paper I**). The experiments were performed using an oxygen pulse response technique, where the flow of oxygen was periodically switched on and off while a constant concentration of methane was flowed over the catalyst. The concentration of oxygen was 1.5 % and the concentration of methane 0.1 %, which gives net-oxidizing periods with a large excess of oxygen and net-reducing periods. XAFS spectra recorded during this periodic oxygen pulsing are shown in Figure 5.1a, the difference between the spectra recorded during the rich and lean periods is clearly seen following the absorption edge. The spectra change periodically and reversibly as a result of the periodic oxygen pulses, which is shown by the colour coded intensity map in Figure 5.1b. Also, the methane conversion changes as a result of the oxygen pulsing (Figure 5.1c), with the highest methane conversion observed at the beginning of the rich period (600 s, 1200 s).

To follow the oxidation of Pd, we plot the intensity of the XAFS spectrum just after the absorption edge, at an energy of 24 370 eV, as a function of time. This region of the spectrum is known as the whiteness region and is commonly used as a semi-quantitative measure of the extent of oxidation. Figure 5.2 shows the XAFS whiteness intensity and the methane conversion from the methane pulse response experiments at 300 and 350 °C.

During the lean periods, with oxygen added to the feed, the conversion of methane increases and simultaneously the whiteness intensity increases. The increasing whiteness intensity indicates that the catalyst becomes more oxidized, towards the end of the lean period, both the whiteness intensity and the methane conversion approaches a steady value, indicating that the catalyst is approaching a steady state in terms of both structure and conversion. There is a higher increase in the whiteness intensity at 350 °C compared to 300 °C, but the methane conversion during the lean periods is similar at about 60 %.

The whiteness intensity also shows that there is a difference in the rate of reduction of palladium when the lean period ends and oxygen is removed from the feed. In the experiment at 300 °C, the whiteness intensity initially decreases slowly when oxygen is removed from the feed and after ca 90 s the decrease continues with a higher rate. At 350 °C, the whiteness intensity decreases rapidly as soon as oxygen is removed from the feed. In both experiments, there is a temporary minimum in the methane conversion when oxygen is removed from the feed. In the experiment at 300 °C, the methane conversion increases after the temporary minimum to approximately the same value as during the lean period, and the methane conversion then decreases in the later parts of the rich period. Similarly, in the experiment at 350 °C the conversion increases after the temporary minimum, but here the conversion is higher than during the lean period at approximately 70 %, and later in the rich period the methane conversion decreases.

To further characterize the catalyst during the rich lean cycling, an EXAFS analysis was performed for spectra representing the reduced catalyst during the rich period and the oxidized catalyst at the end of the lean period. Figure 5.3 shows the EXAFS fits from the rich period at 350 °C, as well as the lean period at 300 and 350 °C. The EXAFS fit in R -space gives information about the neighbouring atoms, although R is not identical to the interatomic distances. The spectrum collected during the rich period at 350 °C

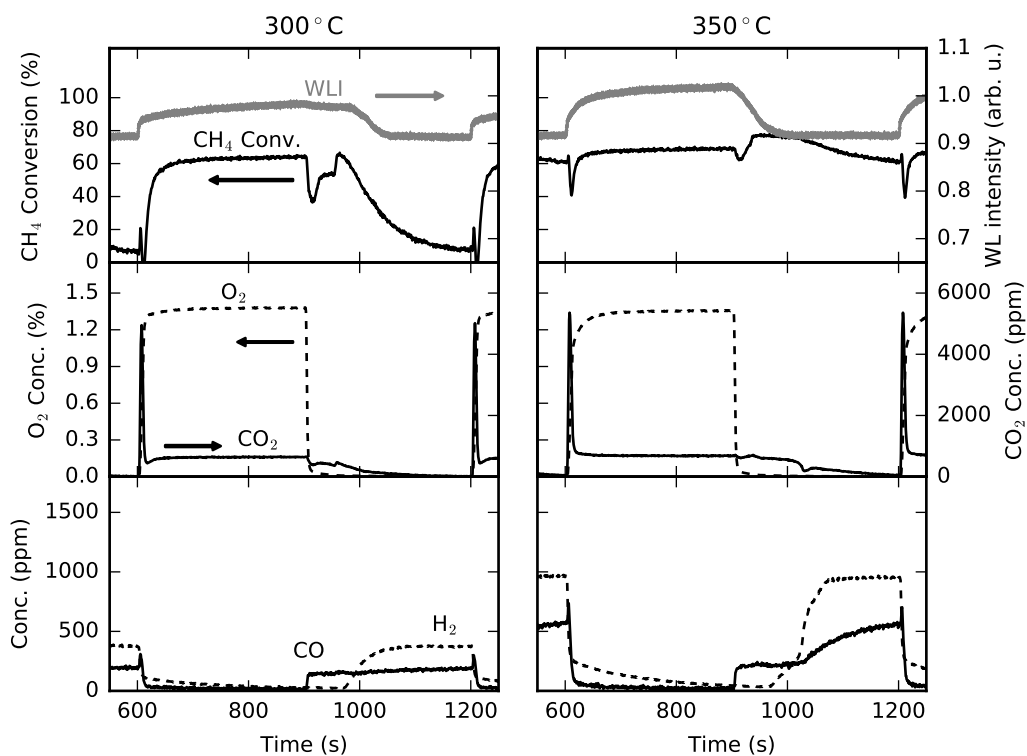


Figure 5.2: Oxidation of 0.1% CH₄ over Pd/Al₂O₃ at 300 and 350 °C, where 1.5% O₂ is introduced for one period. The top panels show the methane conversion and XAFS whiteline at 24372 eV, the middle panels show the O₂ and CO₂ outlet concentrations, and the bottom panels show the CO and H₂ outlet concentrations.

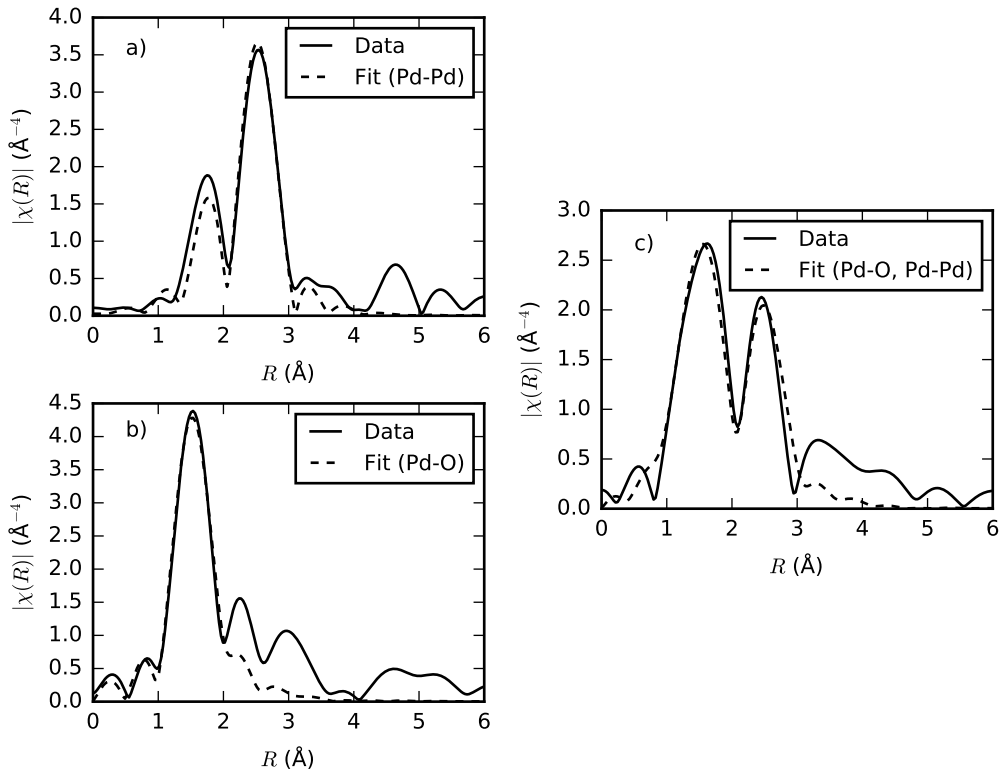


Figure 5.3: EXAFS fits of spectra collected during the a) rich period from the experiment at 350°C, b) lean period from the experiment at 350°C, and c) lean period from the experiment at 300°C.

shows two peaks at $R = 1.7 \text{ \AA}$ and $R = 2.5 \text{ \AA}$, both these peaks are due to the first-shell nearest-neighbour palladium atoms, and the spectrum is similar to that of palladium metal. The spectrum from the lean period at $350 \text{ }^\circ\text{C}$ shows a prominent peak at $R = 1.5 \text{ \AA}$, which is the result of palladium-oxygen bonding, and a similar peak is found in the spectrum from palladium oxide. During the lean period the whiteness intensity in the experiment at $300 \text{ }^\circ\text{C}$ is lower compared to the experiment at $350 \text{ }^\circ\text{C}$, and the EXAFS spectrum is also different. The EXAFS spectrum has strong contribution from both Pd-Pd and Pd-O bonds, indicating an intermediate oxidation state.

The results indicate that at $300 \text{ }^\circ\text{C}$, both the rate of reduction and the oxidation state is lower compared to $350 \text{ }^\circ\text{C}$. The changes in the methane conversion with time on stream can also be connected to the Pd oxidation state. During the lean period the methane conversion approaches a steady value, and when oxygen is removed from the feed at the start of the rich period, the methane conversion decreases. However, after the initial decline, the methane conversion increases for a short period of time, and we attribute this temporary increase in the methane conversion to the reduction of palladium. When oxygen is removed from the feed, the methane conversion decreases but when palladium has been reduced, as indicated by the decreasing whiteness intensity, reduced Pd sites become active for methane dissociation and the conversion increases. Later in the rich periods the methane conversion decreases since oxygen becomes a limiting reactant.

In **Paper I**, the phase sensitive detection technique was used to characterize the Pd catalyst during the rich-lean cycling in order to connect the spectral changes observed with the oxidation and reduction of Pd in the catalyst. To further utilize the potential in this technique a new set of experiments were designed in order to investigate methane oxidation under a wide variety of Pd oxidation states, including low oxidized Pd. These experiments became the basis for **Paper II**, where a methane oxidation was investigated over a Pd/Al₂O₃ catalyst using oxygen pulsing with different oxygen concentrations. In these experiments, a constant flow of 0.1 % methane was maintained over the catalyst while the flow of oxygen was switched on and off every 180 s, three separate experiments were performed using oxygen concentrations of 1.5, 0.25, and 0.15 % oxygen. Figure 5.4 shows the XAFS spectra recorded during the rich and lean periods for the three different experiments at $360 \text{ }^\circ\text{C}$. In the experiment with 1.5 % oxygen the changes in the XAFS spectra between the rich and the lean period are clearly visible, however, in the experiments with lower oxygen concentration the changes in the spectra are fairly small. In order to analyze the changes in the spectra more closely, in particular for the experiments with lower oxygen concentration, the set of XAFS spectra collected were demodulated using the phase sensitive detection technique. A selection of the resulting demodulated spectra for all three experiments is shown in Figure 5.4b. In the demodulated spectra all static features have been removed which clearly shows the energy bands in the spectra that change as a result of the rich-lean cycling. The demodulated spectra can be compared to the Pd-PdO difference spectrum which also shows changes in the same energy bands which shows that the changes in the spectra are due to the oxidation and reduction of palladium.

The methane conversion as a function of time on stream for the experiments with 0.15, 0.25 and 1.5 % oxygen is shown in Figure 5.5 together with the XAFS whiteness intensity. In the experiments with 0.15 and 0.25 % oxygen, the methane conversion is

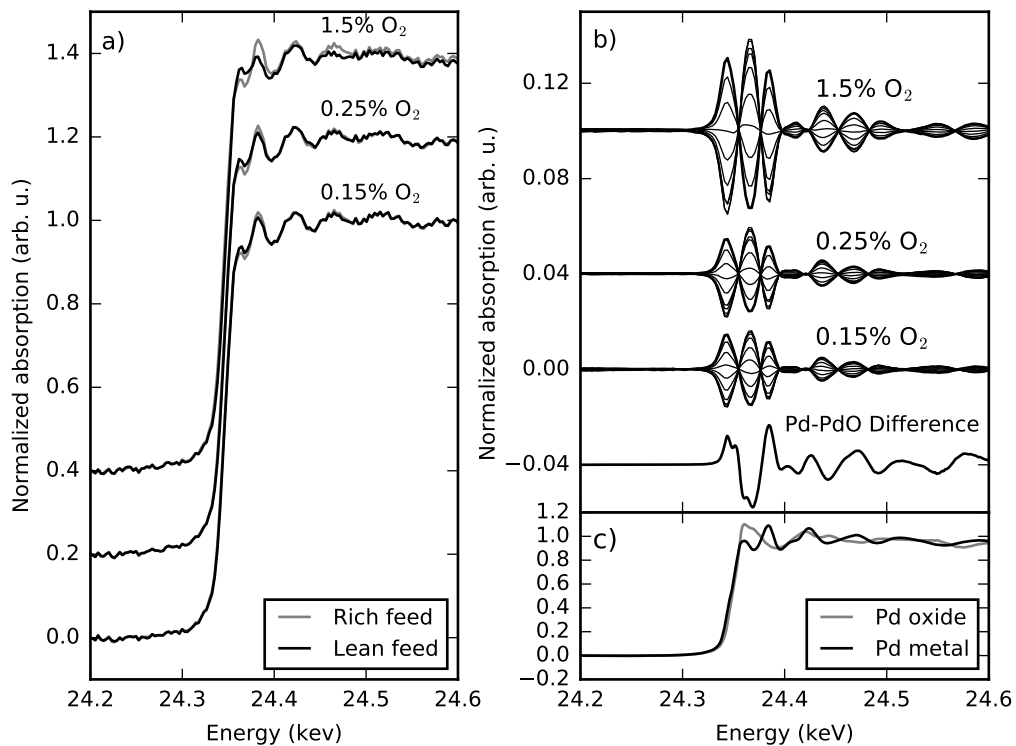


Figure 5.4: (a) XAFS spectra of Pd/Al₂O₃ recorded at the end of the rich and lean periods from the oxygen-pulse experiment with 0.15, 0.25, and 1.5% O₂ at 360 °C. (b) Demodulated XAFS spectra from the experiments with 0.15, 0.25, and 1.5% O₂, and scaled Pd–PdO difference spectrum. (c) XAFS spectra of Pd oxide and Pd metal.

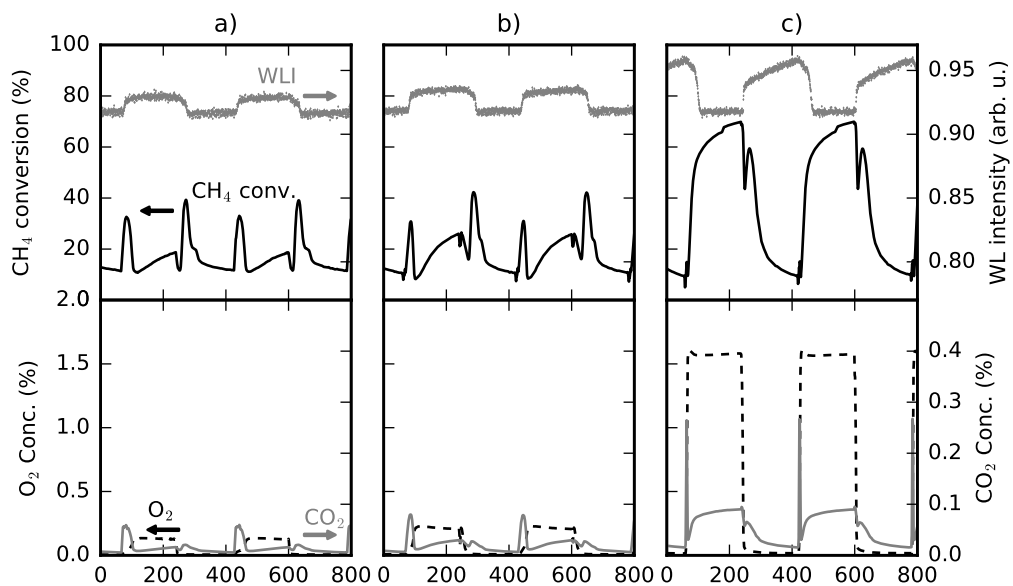


Figure 5.5: Oxidation of 0.1% CH₄ over Pd/Al₂O₃ with 180s oxygen pulses with a concentration of (a) 0.15, (b) 0.25, and (c) 1.5% O₂ at 360 °C. Each panel shows the XAFS whiteline intensity, methane conversion, and the oxygen outlet concentration.

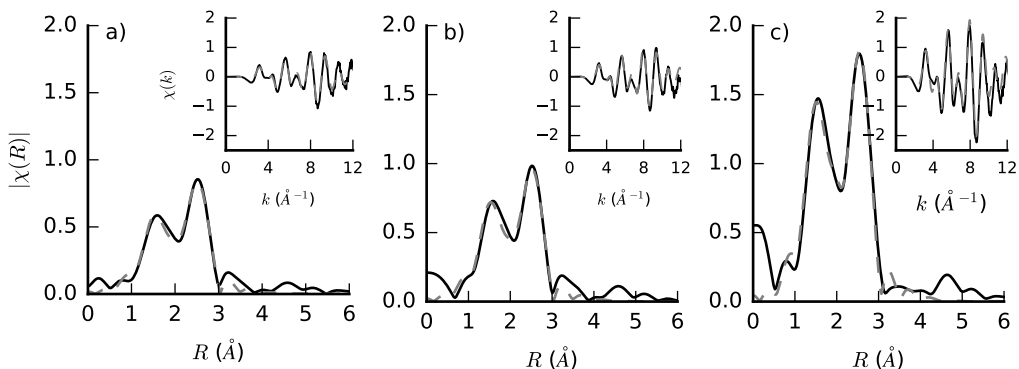


Figure 5.6: k^3 weighted R space and k space (insets) EXAFS functions of demodulated spectra from Pd/Al₂O₃ with (a) 0.15, (b) 0.25, and (c) 1.5 % oxygen pulsing at 360 °C (solid) and fitted curves (dashed).

fairly low but there are temporary increases in the conversion at the switches between the rich and lean periods. In the experiment with 1.5 % oxygen the methane conversion is generally higher, and the highest conversion is observed at the end of the lean period. The whiteline intensity increases rapidly at the start of the lean period in all experiments. When pulsing 0.15 and 0.25 % oxygen the whiteline intensity is stable during the lean period and then decreases rapidly at the start of the next rich period, which gives the whiteline intensity a symmetric profile. In the experiment with 1.5 % oxygen the increase in the whiteline intensity appears to proceed in two steps, after the initial rapid increase there is a slower increase that continues for the duration of the lean period. At the start of the next rich period the whiteline intensity decreases, initially with a slow rate but later the rate increases until a steady value is reached for the rich period.

By using the demodulated spectra from phase sensitive detection we can improve the sensitivity in the EXAFS fitting and also quantify the Pd oxidation state. The demodulated spectra are fitted according to a model where the partially oxidized state during the lean period is fitted as the difference to a reference state. Here, the partially oxidized state is modelled with palladium–oxygen and palladium–palladium bonding, while the reference state includes only palladium–palladium bonding. Figure 5.6 shows the EXAFS fits of the demodulated spectra and Table 5.1 shows the best fit parameters.

The results from the EXAFS fitting show that the change in average Pd–Pd coordination number ($\Delta N_{\text{Pd-Pd}}$) in the lean periods decreases when the oxygen concentration is increased. The average Pd–O coordination number ($N_{\text{Pd-O}}$) increases with higher oxygen concentration, with fitted values of 0.6 ± 0.2 , 0.8 ± 0.2 , and 1.4 ± 0.2 for the lean period in the experiment with 0.15, 0.25, and 1.5 % oxygen. Assuming a mixture of PdO, which has a Pd–O coordination number of 4, and metallic Pd without any Pd–O coordination this corresponds to approximately 15, 20, and 40 % for the experiment with 0.15, 0.25, and 1.5 % oxygen, respectively.

The experiments presented thus far have been based on the pulse-response modulation excitation approach, however, we also wanted to study methane oxidation with step-

Table 5.1: Best-fit parameters for the EXAFS fit of the demodulated spectra from Pd/Al₂O₃ from the experiments with 0.15, 0.25, and 1.5 % oxygen pulsing at 360 °C.

Parameter	Value (0.15% O ₂)	Value (0.25% O ₂)	Value (1.5% O ₂)
$N_{\text{Pd-O}}$	0.6 ± 0.2	0.8 ± 0.2	1.4 ± 0.2
$R_{\text{Pd-O}} (\text{\AA})$	1.991 ± 0.009	1.994 ± 0.008	1.988 ± 0.005
$\sigma_{\text{Pd-O}}^2 (\text{\AA}^2)$	0.007 ± 0.003	0.006 ± 0.003	0.005 ± 0.001
$\Delta N_{\text{Pd-Pd}}$	-0.9 ± 0.3	-1.2 ± 0.4	-3.3 ± 0.5
$\Delta R_{\text{Pd-Pd}} (\text{\AA})$	-0.0089 ± 0.0009	-0.010 ± 0.001	-0.022 ± 0.001
$\Delta \sigma_{\text{Pd-Pd}}^2 (\text{\AA}^2)$	0.0004 ± 0.0003	0.0004 ± 0.0003	-0.0004 ± 0.0005
R -factor	0.011	0.012	0.005

response experiments in order to obtain results at conditions that are steady for longer periods of time. These types of experiments were performed in **Paper III** where a Pd/Al₂O₃ catalyst was held under a flow of 0.2% methane for approximately 15 min after which oxygen was added to the feed. Three different experiments were performed with oxygen concentrations of 0.6, 1.2, and 2.5 %, and each set of experiments were repeated at three different temperatures: 320, 360, and 400 °C. During the experiment, in situ XAFS spectra were recorded as well as the outlet concentrations of reactants and products. Since the experiments were not performed as pulse-response experiments, we cannot use phase sensitive detection to analyze the XAFS results, instead we relied primarily on linear combination fitting to investigate the chemical state of Pd during the experiment.

Figure 5.7 shows the methane conversion and the fraction of Pd²⁺ in the catalyst determined by linear combination fitting as a function of time on stream from the oxygen step-response experiment at 320 °C. The methane conversion decreases to almost zero conversion before oxygen is introduced to the feed, after which the methane conversion increases and full conversion is eventually reached for all three experiments. The fraction of oxidized Pd increases when oxygen is introduced to the feed. The oxidation of Pd appears to be a two step process with an initial rapid oxidation followed by oxidation with a slower rate. We calculated the apparent activation energy for the oxidation of Pd by fitting a straight line to the second part of the oxidized Pd fraction as a function of time, as shown in Figure 5.8a. This results in apparent activation energies of 45, 84, and 101 kJ mol⁻¹ for the experiment with 0.6, 1.2, and 2.5 % oxygen, respectively. The oxidation is likely to be diffusion limited, so these activation barriers do not reflect the thermodynamics of the oxidation process, but rather the dynamics of the oxidation.

Summarizing the results from the operando XAFS studies on Pd/Al₂O₃, the first observation is that the oxidation state of Pd is dependent on the oxygen-to-methane ratio in the feed, and that the oxidation state can change very rapidly, on the order of seconds. We have not performed any detailed analysis of the oxidation-reduction mechanism for Pd under methane oxidation conditions, but some qualitative trends can be observed. Regardless of the oxygen concentration, the initial oxidation of Pd is rapid, and the rapid oxidation is followed by a slower oxidation step. The rate of the second oxidation step depends on the oxygen concentration in the feed as seen for example in Figures 5.5 and 5.7. In Figure 5.5, the oxidation state of Pd hardly increases at all, after the rapid initial oxidation in the two experiments with the lowest oxygen concentration (0.15 %

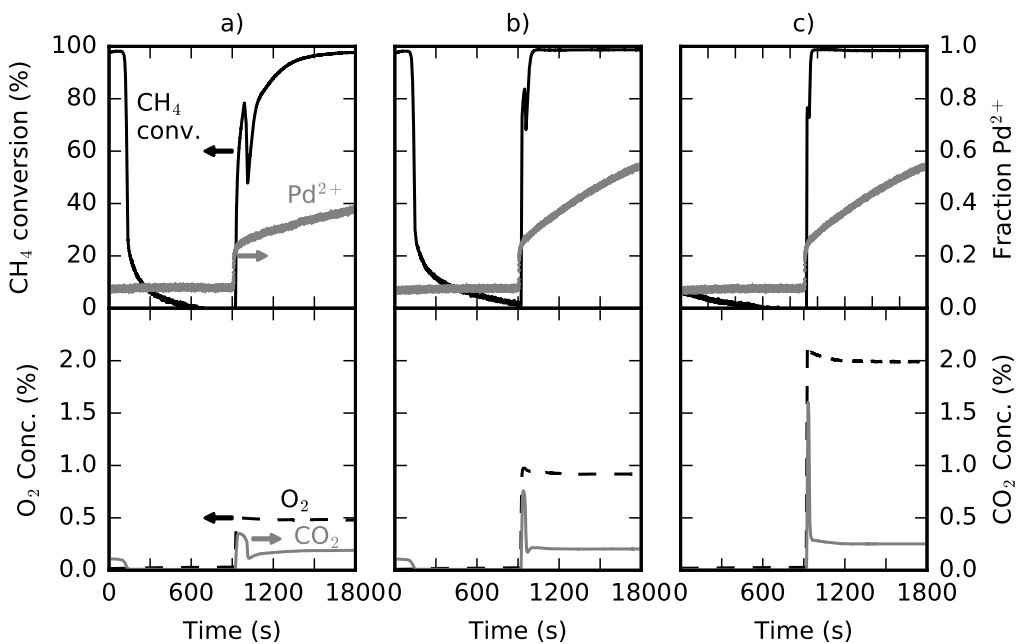


Figure 5.7: Oxidation of 0.2% CH₄ over Pd/Al₂O at 320 °C. Oxygen with a concentration of (a) 0.6, (b) 1.2, and (c) 2.5% is added to the feed at 900s. Each panel shows the fraction of oxidized Pd determined by linear combination fitting, the methane conversion, outlet concentration of oxygen, and outlet concentration of CO₂.

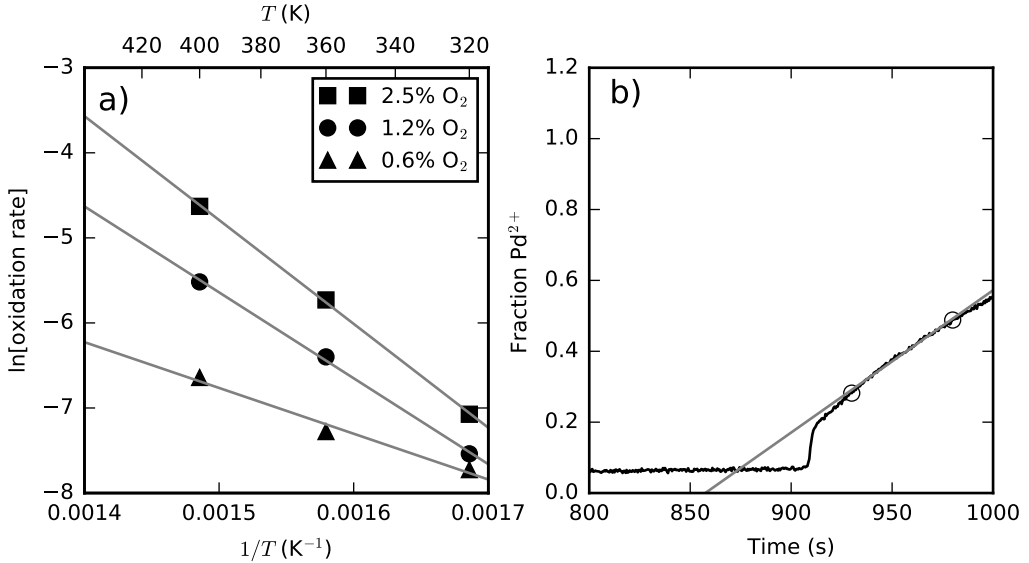


Figure 5.8: a) Arrhenius plot of the fitted oxidation rates in oxygen step-response experiments. b) Fitting the oxidation rate for the experiment with 1.2% O₂ at 400 °C.

O₂/0.1% CH₄ and 0.25% O₂/0.1% CH₄) while for the experiment with the highest oxygen concentration (1.5% O₂/0.1% CH₄) the Pd oxidation state increases almost linearly after the initial rapid oxidation. A similar behaviour can be observed for the reduction of Pd when oxygen is removed from the feed. There is an initial comparatively slow reduction followed by a more rapid reduction until a stable oxidation state is reached under reducing conditions. The oxidation-reduction behaviour observed is consistent with the mechanism proposed by Su et al. [65]. In this mechanism the initial oxidation of Pd is rapid and occurs in accordance with Cabrera-Mott theory. The oxidation is driven by tunneling of electrons through the thin oxide layer which react with adsorbed oxygen to form oxygen anions. The charge separation creates an electric field that drives the anions toward the metal-oxide interface, however, as the thickness of the oxide layer increases the rate of oxidation sharply decreases. Instead, diffusion of oxygen through the oxide layer becomes rate limiting which gives a much slower rate of oxidation [65]. The reduction of PdO is instead nucleation-controlled, where metallic Pd domains must first form which is followed by a rapid reduction with a nearly zero-order dependence on the fraction of reduced Pd [65].

During lean conditions palladium oxide is the active phase for methane oxidation, in all experiments a higher oxidation state of Pd is associated with a higher methane conversion. When oxygen pulsing is performed with different oxygen concentrations (Figure 5.5), the methane conversion increases with the Pd oxidation state, and oxygen is not a limiting reactant since it is detected in the outlet in all experiments. Also in Figure 5.5, in the experiment with the highest oxygen concentration, there is an increase in the methane conversion with time on stream during the lean period, as Pd becomes more oxidized. In

the pulse-response experiments on Pd/Al₂O₃ the methane conversion in many cases go through temporary minima and maxima when oxygen is added or removed from the feed. When oxygen is removed from the feed, the methane conversion typically decreases, and then increases again for a brief period of time, before decreasing again. Similarly, when oxygen is added to the feed the methane conversion increases, and then decreases for a brief period of time, before increasing again. We explain this behaviour by considering the changing surface coverages during the rapid changes in oxygen concentration. When oxygen is removed from the feed, the methane conversion decreases since oxygen vacancies in the PdO lattice are not healed. The reduction of PdO begins with nucleation of metallic Pd domains and this also creates sites where CH₄ can adsorb and oxidize, which briefly increases the methane conversion. Since oxygen has been completely removed from the feed after some time oxygen will become a limiting reactant and the methane conversion will decrease. When oxygen is added to the feed at the start of a lean period the methane conversion increases since oxygen is available for methane oxidation, simultaneously there is also an oxidation of carbonaceous species that have accumulated on the surface of the catalyst during the rich period. The Pd surface will be rapidly oxidized, as indicated by the rapid increase of the XAFS whiteness intensity at the start of the lean period.

Surface oxidation of Pd results in a lower methane conversion, this can be observed transiently in Figure 5.7 where the temporary decrease in the methane conversion when oxygen is added to the feed is connected to the rate of Pd oxidation. In the experiment with the lowest oxygen concentration (0.2 % CH₄/0.6 % O₂), where the rate of Pd oxidation is slower, the transient period with lower methane conversion is much longer compared to the experiment with higher oxygen concentration. Low methane conversion over surface oxidized Pd can also be observed in Figure 5.5 where the conversion during the lean period is much lower in the two experiments with low oxygen concentration compared to the experiment with high oxygen concentration. In these experiments the oxygen concentration is so low (0.15 % and 0.25 % O₂ with 0.1 % CH₄) so the bulk oxidation of Pd is very slow and Pd is mostly surface oxidized, which gives a lower methane conversion compared to the experiment with 1.5 % O₂ where Pd is bulk oxidized. These findings are also consistent with the much higher apparent activation barrier for methane oxidation reported for oxygen saturated Pd⁰ surfaces (158 kJ mol⁻¹) compared to bare Pd metal or PdO (84 and 61 kJ mol⁻¹, respectively) [66]. Palladium readily forms surface oxides under oxidizing conditions, the ($\sqrt{5} \times \sqrt{5}$)R27° surface oxide which forms over Pd(100), was reported not to be very active for methane oxidation, compared to a thicker bulk-like PdO film [57].

Support effects

The operando XAFS studies in this thesis were mostly performed with Pd/Al₂O₃ catalysts, however, in **Paper I** also experiments with Pd/CeO₂ were included. γ -Al₂O₃ is commonly used as a catalyst support material due to its high surface area and thermal stability. Furthermore, for XAFS studies Al₂O₃ supports have the advantage that aluminium and oxygen are light elements compared to most noble metals, which reduces scattering of the X-rays. Cerium on the other hand is a heavy element ($Z = 58$) that scatters X-rays more

effectively than lighter elements, and a high cerium content in the catalyst will make it difficult to record high quality XAFS spectra.

In our experiments with Pd/CeO₂, we were able to record the part of the XAFS spectrum close to the absorption edge and thus compare the evolution of the whiteline intensity with the Pd/Al₂O₃ catalyst as a function of time on stream. Figure 5.9 shows the whiteline intensity recorded during the rich-lean cycling experiments as well as the methane conversion and outlet concentrations of products and reactants. The oxidation of Pd supported on CeO₂ is quicker compared to Pd/Al₂O₃, and the reduction of Pd when oxygen is removed from the feed is also slower. This observation is consistent with previous reports that CeO₂ helps to stabilize Pd in the oxidized state [67]. There are also some interesting differences in the methane conversion and outlet product concentrations. The methane conversion increases rapidly when oxygen is removed from the feed and at the same time the outlet concentrations of H₂ and CO increase. This indicates that the catalyst can rapidly switch to methane conversion by partial oxidation, when the oxygen concentration in the feed decreases. This difference might be related to the oxygen storage capability of CeO₂ and increased oxygen mobility, leading to reverse spillover of oxygen to Pd [68]. These results indicate that the support material can help to stabilize Pd in the oxidized state and maintain high methane conversions in oxygen deficient feeds, which would be an important function in automotive catalysis.

Bimetallic Pt-Pd catalysts

Bimetallic catalysts have a widespread use in chemical processes such as catalytic reforming, pollution control, and energy conversion. Combining two metals as the active phase can lead to higher catalytic activity and selectivity, compared to the monometallic counterparts, which makes bimetallic catalysts an important class of catalysts. For the total oxidation of methane, Pd–Pt catalysts is a bimetallic catalyst system of particular interest. Previous studies have reported that supported Pd–Pt catalysts show an increase in CH₄ oxidation activity with time on stream and have higher long-term stability than supported Pd catalysts [69–72]. Moreover, Pd–Pt catalysts have been reported to be less prone to sintering in oxidative environment compared to Pt only catalysts [73]. The structure of the metallic phase of the Pt–Pd catalyst is likely to be complex, alloy formation between Pd and Pt along with segregation of Pd to the surface has been previously reported [74–76]. In the present study, we wanted to investigate how the calcination condition and oxidative and reductive treatment influence the surface composition and alloy formation of model Pd–Pt/Al₂O₃ catalysts. Furthermore, we also wanted to investigate how the structure and composition of Pd–Pt/Al₂O₃ catalyst affect the methane oxidation activity. Pd–Pt/Al₂O₃ catalysts were investigated in two different studies, the first study (**Paper IV**) focused on characterizing the metal particles during oxidation/reduction, while the second study (**Paper V**) investigated methane oxidation during rich-lean cycling with operando DRIFTS/MS and in situ XAFS. The catalysts used in these studies were prepared by incipient wetness impregnation with a Pd loading of 2.0% and Pt loading of 0.4%. Three different catalysts were prepared by calcination under three different conditions, in air at 500 °C for 2 h (denoted F500), in air at 800 °C for 10 h (F800), and

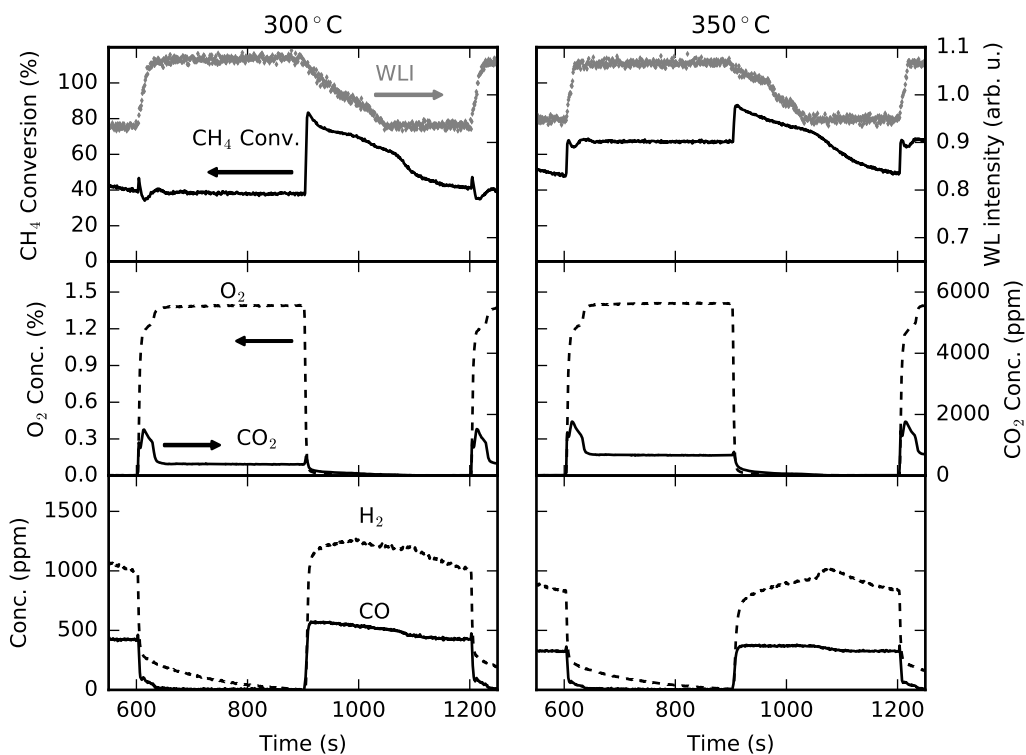


Figure 5.9: Oxidation of 0.1% CH₄ over Pd/CeO₂ at 300 °C and 350 °C, with 1.5% O₂ introduced for one period. The top panel shows the CH₄ conversion and XAFS whiteline intensity at 24372 eV; the second panel shows the outlet concentration of O₂ and CO₂; and the third panel shows the outlet concentrations of H₂ and CO.

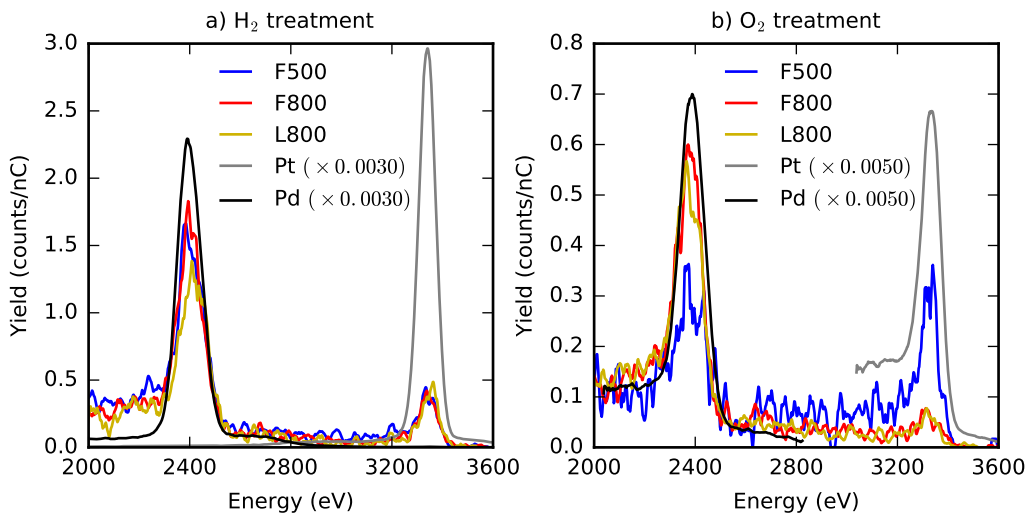


Figure 5.10: LEIS results for (a) the reduced (50 mbar of H₂ at 300 °C for 25 min) and (b) oxidized (atomic oxygen at room temperature for 60 min) Pd–Pt/Al₂O₃ catalysts. Pd and Pt are included as references.

in air with addition of 10% water at 800 °C for 10 h (L800). The as-prepared catalysts were characterized using TEM, XRD, and CO chemisorption.

The TEM analysis of the F500 sample showed that larger Pt nanoparticles (up to about 100 nm) were present mainly outside the alumina matrix, while significantly smaller Pd nanoparticles were embedded in the alumina matrix. By mapping the elemental distribution using energy-dispersive spectroscopy in TEM only segregated palladium and platinum nanoparticles could be detected for the Pd–Pt F500 catalyst. For the F800 sample the morphology of the catalyst is different, since Pt is alloyed with Pd and the particles are situated mainly in the alumina matrix. The Pt–Pd nanoparticles have a diameter of about 50–100 nm and in addition a large number of smaller Pd nanoparticles (about 5 nm diameter) can be observed well distributed across the alumina support. The morphology of the L800 Pd–Pt catalyst was similar to the F800 counterpart, however, the Pd–Pt nanoparticles appeared to have a more uniform size with a diameter of around 50 nm. The XRD pattern for the Pd–Pt F500 catalyst showed reflections from PdO, but not from metallic Pd or Pt, likely Pt could not be observed due to the relatively low Pt loading and/or high Pt dispersion. For the F800 and L800 Pd–Pt catalysts reflections for PdO as well as metallic *fcc* structure could be observed, the *fcc* reflections were sharp indicating a bulk structure and were observed at angles in between those expected for metallic Pd and Pt, indicating the formation of an alloy.

The characterization results for the as-prepared catalysts show that while the F800 and L800 Pd–Pt catalysts feature alloyed Pd–Pt nanoparticles, the F500 catalysts contain mainly segregated Pd and Pt nanoparticles. To investigate how this difference affects the oxidation and reduction behaviour, oxidation and reduction were studied using low-energy ion scattering (LEIS) and in situ XAFS. Figure 5.10 shows the surface composition

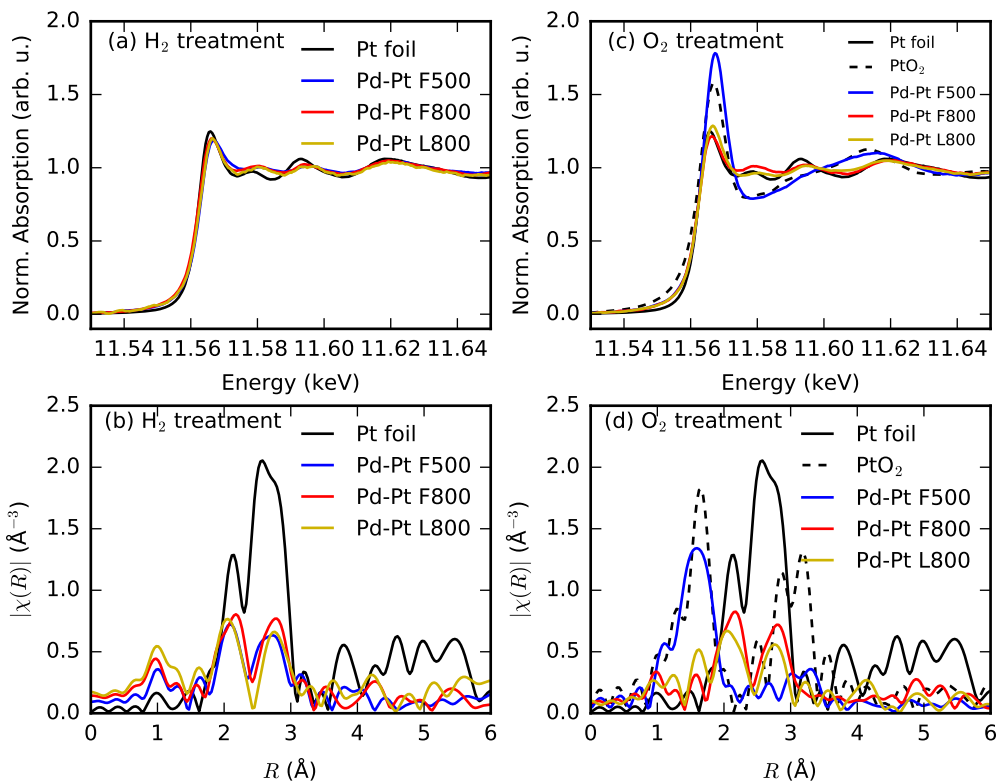


Figure 5.11: Pt L_{III} edge in situ XAFS spectra of the reduced (a, b) and oxidized (c, d) Pd–Pt/ Al_2O_3 catalysts at 300 °C. Pt foil and PtO_2 spectra are included as references. (a, c) XANES spectra and (b, d) Fourier transformed EXAFS spectra (magnitude with k -weight = 2).

determined by LEIS for the three Pt–Pd bimetallic catalysts. Under reducing conditions both Pd and Pt are exposed on the surface of the catalyst with Pd being the dominating species. The surface Pd/Pt atomic ratio is in the range 3.9–4.8 for all catalysts, which shows that Pt is enriched at the surface compared to the bulk. After oxidizing treatment a distinct difference is observed between the F500 catalyst, and the F800 and L800 catalysts. For the F500 catalysts approximately the same amounts of Pd and Pt are exposed at the surface, while for the F800 and L800 samples the surface becomes highly enriched with Pd, the surface Pd/Pt atomic ratio is 17.2 and 16.3 for the F800 and L800 catalyst, respectively. It is expected that under oxidizing conditions Pd is oxidized and forms PdO which dominates the surface.

To further study oxidation and reduction of the catalysts, in situ XAFS was recorded during transient oxidation and reduction at both the Pd K-edge and the Pt L_{III} edge. The changes in the Pd K-edge XAFS spectra during oxidation are consistent with the formation of PdO , and Pd was reduced to metallic Pd after treatment in hydrogen.

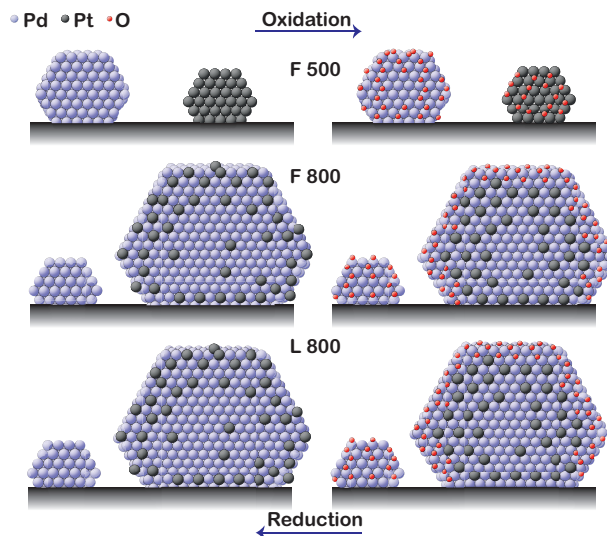


Figure 5.12: Illustration of the mechanism proposed for the oxidation and reduction of the different Pd–Pt catalysts. REPRINTED WITH PERMISSION FROM REFERENCE [77]. COPYRIGHT 2016 AMERICAN CHEMICAL SOCIETY.

There was no direct observation of Pd–Pt bonding in the Pd K-edge XAFS for the F800 and L800 catalysts, but this might be due to the low loading of Pt compared to Pd. Figure 5.11 shows the Pt L_{III} edge XAFS spectra after oxidation in 5% O₂ for 20 min and after reduction in 5% H₂ for 20 min. The XANES spectra for the reduced catalysts are all similar to the Pt foil spectrum, indicating that Pt is in a metallic state. For the oxidized catalysts the F500 catalyst has a much higher whiteline intensity, giving a spectrum similar to that of PtO₂ while the spectra for the F800 and L800 samples are similar to Pt foil. This result suggests that Pt in the F500 catalyst is in a state with high affinity to oxygen, possibly in the form of small Pt nanoparticles, that are readily oxidized. The Fourier transforms of the EXAFS spectra for the reduced catalysts show a double peak structure at *R* values between 2 and 3 Å, which is attributed to metal-metal scattering. The peak positions for the F500 sample are similar to those of Pt foil, indicating a Pt–Pt type bond, while for the F800 and L800 catalysts the peaks are shifted to slightly higher *R* values suggesting a Pt–M type bond (M = Pd or Pt). The Fourier transformed EXAFS spectra for the oxidized F800 and L800 catalysts are very similar to those recorded for the reduced catalyst, this shows that Pt in the catalysts retain its metallic state after treatment in oxygen.

Summarizing the results from the characterization of the as-prepared catalysts as well as the LEIS and XAFS experiments, there is clear evidence of alloy formation between Pd and Pt in the catalysts calcined at 800 °C. In contrast, for the catalyst calcined at 500 °C, no similar evidence is found indicating alloying between Pd and Pt. Furthermore, the F500 catalyst shows a distinctly different behaviour under oxidation, as seen both in the LEIS and in situ XAFS experiments. The Pt L_{III} edge XAFS for the F500 catalyst shows that Pt in the catalyst is oxidized when treated in oxygen, while for the F800 and

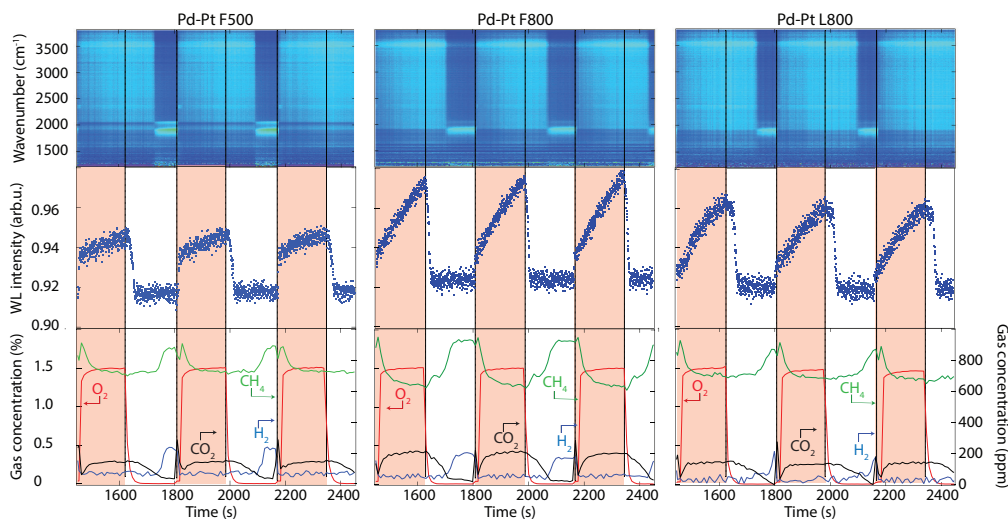


Figure 5.13: Oxidation of 0.1% CH₄ over the Pd–Pt/Al₂O₃ F500 (left panels), Pd–Pt/Al₂O₃ F800 (middle panels), and Pd–Pt/Al₂O₃ L800 (right panels) samples, with periodic pulsing of 1.5% O₂. The top panels show the color coded intensities (blue low intensity, red high intensity) of the IR absorption bands in the region 1200–3800 cm⁻¹. The middle panels show the evolution of the XAFS whiteline intensity (WLI) at 24 372 eV. The bottom panels show the outlet concentration of O₂ (red), CO₂ (black), CH₄ (green) and H₂ (blue) measured by MS.

L800 catalysts Pt is in a metallic state also after oxidation. We do not find any evidence of a mixed Pt–Pd metal oxide in any of the catalysts. The EXAFS analysis for the F500 sample shows both PdO and PtO₂ after the in situ oxidation, however, if the nanoparticles were mixed Pd–Pt we would expect to see some indication of alloy formation, similar to what is observed for the F800 and L800 catalysts. This leads us to exclude the formation of a mixed Pt–Pd oxide on all samples. The Pt L_{III} edge EXAFS analysis of the F800 and L800 catalysts reveals Pd–Pt bonding, while the Pd K edge EXAFS reveals mostly PdO bonding. This suggests that there are regions containing mostly Pd, as well as regions with Pd–Pt mixing. Under reducing conditions, the bimetallic nanoparticles expose a Pd–Pt metallic surface enriched in Pt, while under oxidizing conditions PdO dominates the surface. PdO is present both in form of crystals at the surface of the Pd–Pt particles and as isolated PdO crystals on the support. For the F500 catalyst, Pd and Pt are found as individual monometallic nanoparticles that are oxidized to PdO and PtO_x during oxidizing conditions. Figure 5.12 shows an illustrative model for the oxidation and reduction behaviour of the Pd–Pt catalysts.

The methane oxidation activity of the Pd–Pt catalysts was investigated using operando DRIFTS/MS and in situ XAFS. The experiments were performed as pulse-response experiments with pulses of 1.5% O₂ introduced over a constant flow of methane of 0.1% with a duration of three minutes at a temperature of 360 °C. The operando DRIFTS/MS

experiment was combined with in situ energy-dispersive XAFS at the Pd K edge, recorded under the same conditions. The results from these experiments for the Pd–Pt F500, F800, and L800 catalysts are summarized in Figure 5.13. The evolution of the IR absorption bands during the rich-lean cycling shows an increased absorption in the region 1800–2000 cm^{-1} at the end of the rich periods corresponding to the adsorption of carbonyls (CO adsorbed on the metal nanoparticles). For the F500 catalyst two distinct bands are observed in this range, with linearly adsorbed carbonyls giving a band at higher wavenumbers and bridge bonded carbonyls giving a band at lower wavenumbers. For both the F800 and L800 catalysts, bridge bonded carbonyls appear to be dominating since the band at higher wavenumbers is much less intense. The difference in the carbonyl absorption bands suggests that the surface composition is different between the F500 catalyst with monometallic Pd and Pt particles, compared to the F800 and L800 catalysts, which contain alloy Pd–Pt nanoparticles. The whiteline intensity of the Pd K edge is used to follow the changes in the oxidation state of Pd, as was done in earlier studies. The increasing whiteline intensity during the lean periods indicates an oxidation of Pd and the whiteline intensity decreases rapidly at the start of the rich period. The rate of oxidation is higher for the F800 and L800 catalysts, compared to the F500 catalyst. This suggests that the alloyed nanoparticles follow different oxidation kinetics compared to monometallic nanoparticles during methane oxidation, this could be caused by the alloying but possibly also by differences in particle size distribution or shape. Comparing the methane oxidation activity for the three catalysts we find that the F800 and L800 catalysts, containing alloyed nanoparticles, have higher activity than the F500 catalyst, containing monometallic nanoparticles. This may be due to the increased amount of PdO for the catalysts with alloyed nanoparticles, which is indicated by the increased whiteline intensity in Figure 5.13. However, there is also a difference in activity between the F800 and L800 samples, but the cause of this is not clear. One possible explanation for this observation is that the F800 sample features a smaller average particle size than the L800 sample which results in the formation of a higher amount of PdO. This is beneficial for the methane oxidation reaction but to analyze this in more depth would require an accurate particle size distribution which is presently not available. Overall, we find that high activity for methane oxidation in Pt–Pd bimetallic catalysts is associated with the formation of PdO on the surface of the catalyst, similar to the results found for Pd-only catalysts.

Simulated XAFS spectra from first principles

In addition to the experimental operando spectroscopy studies, we have also investigated theoretical simulations of XANES spectra from first principles. XANES spectra of palladium model systems were calculated using the FEFF code, using structures with geometries optimized using density functional theory. The palladium model systems were chosen in order to investigate the effect of morphology, particle size, and oxidation state on the Pd K edge XANES spectra. The results showed that the morphology of a Pd nanoparticle has a limited impact on the XANES spectra, for example nanoparticles of similar size with different morphologies were very similar. Pd nanoparticles with different

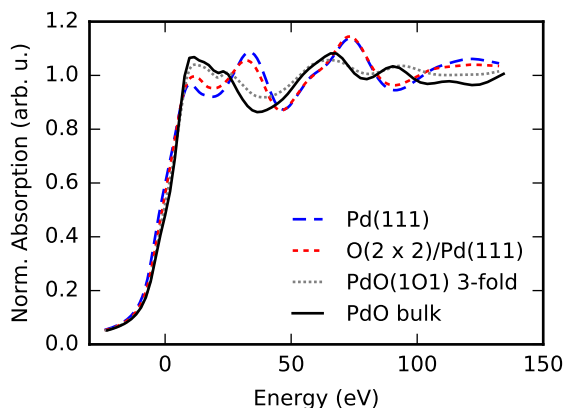


Figure 5.14: Pd K edge XANES spectra simulated using FEFF9 for a palladium atom forming an fcc hollow in the Pd(111) surface, the corresponding atom with a (2 x 2) oxygen overlayer (coverage 0.25 ML), the threefold coordinated surface Pd in PdO(101), and bulk PdO.

particle sizes produced spectra that were somewhat different, mainly owing to the different Pd–Pd nearest neighbor distances resulting in shifted peak positions on the energy axis, as well as differences in the average number of nearest neighbors which affected the amplitude of the XAFS oscillations. The effect of Pd oxidation state can be seen in the simulated XANES spectra shown in Figure 5.14. The spectrum for palladium at the Pd(111) surface is similar to the spectrum of bulk metal. Adding an O(2 x 2) overlayer gives an increased amplitude of the first peak after the absorption edge and a decreased amplitude in the second peak. The PdO(101) surface of bulk PdO features Pd with a 3-fold oxygen coordination as well as Pd with a 4-fold oxygen coordination, the spectrum for the 3-fold coordinated surface atom as well as the spectrum for the PdO bulk (4-fold oxygen coordination) are shown in Figure 5.14. The spectrum of the PdO bulk and PdO surface atoms are similar, however the amplitude of the XAFS oscillations is lower for the PdO(101) surface atom.

Chapter 6

Conclusions and Outlook

In this thesis we have explored the use of operando XAFS spectroscopy with focus on Pd catalysts for the total oxidation of methane. Although many interesting results have been obtained, in science there is always a drive to refine procedures and techniques in order to further advance knowledge. In the field of operando XAFS both experimental techniques and equipment, as well computation and simulation of XAFS data, are areas in which future developments are expected to make a large impact.

To obtain the results presented in this thesis we have primarily relied on the ability of XAFS to provide information on the chemical composition of the active phase in the catalyst. Moreover, XAFS spectra were acquired with high time resolution under in situ conditions. By using these techniques we have been able to show several results of how the active phase of Pd catalysts changes under reaction conditions for methane oxidation. Another interesting result is the rate of oxidation and reduction of palladium when the reaction conditions change. Although it is difficult to extract kinetic parameters for these catalysts with a heterogeneous structure, the results highlight the rapid rate with which the Pd oxidation state can change.

One piece of information that is mostly missing from XAFS is information specifically on the surface structure of palladium. In this thesis we have worked with experimental and data processing techniques in order to improve the sensitivity to small changes in the XAFS spectra, primarily by using modulation excitation spectroscopy and phase sensitive detection. Using these techniques we have been able to refine and expand the results obtained from the collected spectroscopic data and examine the palladium phase in more detail. XAFS will probably never approach the surface sensitivity of techniques like XPS, but with additional improvements, in situ XAFS can become a much more sensitive technique to small changes in the active phase, for example, changes that are localized to the surface.

Next steps

In this thesis one theoretical study was performed focusing on first-principles simulations of XANES spectra. The results from this study showed that the changes in the XANES

spectra just from the adsorption of oxygen on the Pd surface are fairly limited, a local structure similar to bulk PdO is necessary to have a strong whitenline peak. Although this study was limited in its scope, it highlights the capabilities of current techniques of simulating the full XAFS spectrum, and with future developments and higher availability of these techniques they have a strong potential to make a larger impact in catalysis research. However, our experience so far indicates that in order to achieve tight integration between theory and experiments, carefully designed experiments and suitable model catalysts are required.

The experimental operando spectroscopy studies in this thesis were mainly performed with the energy-dispersive XAFS technique. The advantage with this technique is that spectra can be acquired very quickly, and in our experiments we have been able to achieve time resolutions as low as 200 ms. This time-resolution is certainly sufficient for operando catalysis experiments, but the energy-dispersive technique comes with significant sacrifices in spectral resolution. From this perspective, further developments in XAFS techniques should focus on achieving higher spectral quality at in situ/operando conditions. During the work with this thesis there was no opportunity to perform experiments with high time resolution quick XAFS, but for operando catalysis I would think this technique has more potential for the future. Another area where development can make advances is sample cells for operando experiments. The sample cell has to be designed so that kinetic data can be measured and simultaneously high-quality spectra can be recorded. In addition to optimizing and balancing these two requirements there is also a need for sample cells that are compatible with more than one characterization technique, such as XAFS and XRD, or XAFS and DRIFTS. Although this is becoming increasingly available at XAFS beamlines, there is always a balance between increasing the complexity of the experiment, and the additional data that can be gained. The increasing complexity of experiments performed at synchrotron beamlines makes it essential to have a good collaboration between beamline scientists and the research groups that are granted time to use the beamline.

Outlook

The results obtained so far for the total oxidation of methane over Pd catalysts highlight the rapid oxidation and reduction of Pd when the feed gas composition changes and that maintaining Pd in a bulk-oxidized state is important to maintain high conversion. The experiments with Pd/CeO₂ show that ceria is capable of stabilizing Pd in its oxidized state. Further work should be aimed at investigating more complex multi-component support materials, such as CeO₂ combined with Al₂O₃ and additional dopants to find out how different support materials affect properties of the catalyst such as catalytic activity and stability. Including platinum in the palladium active phase gives beneficial properties to the catalyst, such as increased long-term stability. However, our work shows that the synthesis procedure, and in particular the calcination temperature, is important to obtain alloying between Pt and Pd. Our results for methane oxidation over Pd–Pd/Al₂O₃ indicate that PdO is still the component that is responsible for most of the methane oxidation activity and further investigations could be aimed at further

characterize catalysts with different Pd/Pt atomic ratios. Pd–Pt catalysts can also be suitable systems for further theoretical studies, both with respect to electronic structure and how this affects the catalytic activity, and also how the interaction between Pt and Pd affects the XAFS spectrum. Operando XAFS has been a critical tool in order to obtain the results in this thesis, although limited to synchrotron radiation facilities, with continuous improvements in procedures and techniques operando XAFS will be an important technique in catalysis research for many years in the future.

Chapter 7

Acknowledgements

The research in this thesis was carried out at the division of Applied Chemistry and at the Competence Centre for Catalysis (KCK), Chalmers University of Technology, Gothenburg, Sweden, during the period September 2013 to December 2017.

The Competence Centre for Catalysis is hosted by the Chalmers University of Technology and financially supported by the Swedish Energy Agency and the member companies AB Volvo, ECAPS AB, Haldor Topsøe A/S, Scania CV AB, Volvo Car Corporation AB and Wärtsilä Finland Oy.

This research has been funded by the Swedish Research Council (Vetenskapsrådet) in the project “Unravelling catalytically active sites with X-ray absorption spectroscopy”. Also, beam time granted at ESRF and MAXLAB, as well as CPU time granted by SNIC at C3SE is gratefully acknowledged.

I would also like to thank:

My main supervisor Magnus Skoglundh for all the support and guidance, and for always encouraging me to develop as a researcher. My co-supervisors Per-Anders Carlsson and Henrik Grönbeck for always taking the time to help me with my scientific questions, big as well as small.

My examiner and head of division Anders Palmqvist for creating such a nice working atmosphere at the division, and Frida Andersson for helping out with small and big issues of all different types.

Natalia, Emma, Sheedeh, Peter and Ting for the nice scientific collaboration as well as all present and former colleagues at Applied Surface Chemistry, and the Competence Centre for Catalysis.

My parents, my brothers, and my grandparents for always being there for me.

References

- [1] T. Korakianitis, A. Namasivayam, and R. Crookes. Natural-gas fueled spark-ignition (SI) and compression-ignition (CI) engine performance and emissions. *Progress in Energy and Combustion Science* **37.1** (2011), 89–112. DOI: 10.1016/j.pecs.2010.04.002.
- [2] A. R. Brandt, G. A. Heath, E. A. Kort, F. O’Sullivan, G. Petron, S. M. Jordaan, P. Tans, J. Wilcox, A. M. Gopstein, D. Arent, S. Wofsy, N. J. Brown, R. Bradley, G. D. Stucky, D. Eardley, and R. Harriss. Methane Leaks from North American Natural Gas Systems. *Science* **343.6172** (2014), 733–735. DOI: 10.1126/science.1247045.
- [3] P. Weiland. Biogas production: current state and perspectives. *Applied microbiology and biotechnology* **85.4** (2010), 849–860. DOI: 10.1007/s00253-009-2246-7.
- [4] A. Myhre, D. Shindell, F.-M. Bréon, W. Collins, J. Fuglestvedt, J. Huang, D. Koch, J.-F. Lamarque, D. Lee, B. Mendoza, T. Nakajima, A. Robock, G. Stephens, T. Takemura, and H. Zhang. “Anthropogenic and Natural Radiative Forcing”. *Climate Change 2013: The Physical Science Basis. Contribution of Working Group I to the Fifth Assessment Report of the Intergovernmental Panel on Climate Change*. Ed. by T. Stocker, D. Qin, G.-K. Plattner, M. Tignor, S. Allen, J. Boschung, A. Nauels, Y. Xia, V. Bex, and P. Midgley. Cambridge, United Kingdom and New York, NY, USA: Cambridge University Press, 2013.
- [5] R. Burch and P. K. Loader. Investigation of Pt/Al₂O₃ and Pd/Al₂O₃ catalysts for the combustion of methane at low concentrations. *Applied Catalysis B: Environmental* **5.1-2** (1994), 149–164. DOI: 10.1016/0926-3373(94)00037-9.
- [6] G. Ertl. Reactions at Surfaces: From Atoms to Complexity (Nobel Lecture). *Angewandte Chemie International Edition* **47.19** (2008), 3524–3535. DOI: 10.1002/anie.200800480.
- [7] H.-J. Freund, H. Kuhlenbeck, J. Libuda, G. Rupprechter, M. Bäumer, and H. Hamann. Bridging the pressure and materials gaps between catalysis and surface science: clean and modified oxide surfaces. *Topics in Catalysis* **15.2/4** (2001), 201–209. DOI: 10.1023/A:1016686322301.
- [8] P. Stoltze and J. K. Nørskov. Bridging the “pressure gap” between ultrahigh-vacuum surface physics and high-pressure catalysis. *Physical Review Letters* **55.22** (1985), 2502–2505. DOI: 10.1103/PhysRevLett.55.2502.
- [9] M. A. Bañares. Operando methodology: Combination of in situ spectroscopy and simultaneous activity measurements under catalytic reaction condition. *Catalysis Today* **100.1-2** (2005), 71–77. DOI: 10.1016/j.cattod.2004.12.017.

- [10] J. A. Rodriguez, J. C. Hanson, and P. J. Chupas. "Goals and Challenges for the In-situ Characterization of Heterogeneous Catalysts". *In-situ Characterization of Heterogeneous Catalysts*. Ed. by J. A. Rodriguez, J. C. Hanson, and P. J. Chupas. Hoboken, New Jersey: John Wiley & Sons Inc., 2013, pp. 1–22.
- [11] B. M. Weckhuysen. "Ultraviolet-Visible Spectroscopy". *In-situ Spectroscopy of Catalysts*. Ed. by B. M. Weckhuysen. American Scientific Publishers, 2004, pp. 255–270.
- [12] T. Okawa, T. Onishi, and K. Tamaru. Infrared and Kinetic Study of Ammonia Decomposition on Supported Iron Catalysts: Infrared Observation of Molecularly Adsorbed N₂ in Ammonia Decomposition. *Zeitschrift für Physikalische Chemie* **107.2** (1977), 239–243. DOI: 10.1524/zpch.1977.107.2.239.
- [13] J. W. Niemantverdriet. *Spectroscopy in Catalysis: An Introduction*. 3rd ed. Weinheim: Wiley-VCH Verlag GmbH & Co. KGaA, 2007.
- [14] J. R. Anderson and K. C. Pratt. *Introduction to characterization and testing of catalysts*. Academic Press, 1985.
- [15] D. E. Starr, H. Bluhm, Z. Liu, A. Knop-Gericke, and M. Hävecker. "Application of ambient-pressure X-ray photoelectron spectroscopy for the in-situ investigation of heterogeneous catalytic reactions". *In-situ Characterization of Heterogeneous Catalysts*. Ed. by J. A. Rodriguez, J. C. Hanson, and P. J. Chupas. Hoboken, New Jersey: John Wiley & Sons, Inc., 2013, pp. 315–343.
- [16] D. E. Starr, Z. Liu, M. Hävecker, A. Knop-Gericke, and H. Bluhm. Investigation of solid/vapor interfaces using ambient pressure X-ray photoelectron spectroscopy. *Chemical Society Reviews* **42.13** (2013), 5833. DOI: 10.1039/c3cs60057b.
- [17] S. Alayoglu and G. A. Somorjai. Ambient Pressure X-ray Photoelectron Spectroscopy for Probing Monometallic, Bimetallic and Oxide-Metal Catalysts under Reactive Atmospheres and Catalytic Reaction Conditions. *Topics in Catalysis* **59.5-7** (2016), 420–438. DOI: 10.1007/s11244-015-0534-2.
- [18] R. Sharma and P. A. Crozier. "Environmental Transmission Electron Microscopy in Nanotechnology". *Handbook of Microscopy for Nanotechnology*. Ed. by N. Yao and Z. L. W. Kluwer Academic Publishers, 2005.
- [19] P. L. Gai, R. Sharma, and F. M. Ross. Environmental (S)TEM Studies of Gas-Liquid-Solid Interactions under Reaction Conditions. *MRS Bulletin* **33.02** (2008), 107–114. DOI: 10.1557/mrs2008.23.
- [20] A. Frennet and C. Hubert. Transient kinetics in heterogeneous catalysis by metals. *Journal of Molecular Catalysis A: Chemical* **163.1-2** (2000), 163–188. DOI: 10.1016/S1381-1169(00)00385-X.
- [21] J. Happel. Transient tracing. *Chemical Engineering Science* **33.11** (1978), 1567. DOI: 10.1016/0009-2509(78)85214-2.
- [22] C. O. Bennett. "Understanding Heterogeneous Catalysis Through the Transient Method". *Catalysis Under Transient Conditions*. Ed. by A. T. Bell and L. L. Hegedus. American Chemical Society, 1982, pp. 1–32. DOI: 10.1021/bk-1982-0178.ch001.
- [23] P. Biloen. Transient kinetic methods. *Journal of Molecular Catalysis* **21.1-3** (1983), 17–24. DOI: 10.1016/0304-5102(93)80108-7.

- [24] A. Machocki, M. Rotko, and B. Stasinska. SSITKA studies of the catalytic flameless combustion of methane. *Catalysis Today* **137**.2-4 (2008), 312–317. DOI: 10.1016/j.cattod.2007.11.027.
- [25] P.-A. Carlsson, M. Skoglundh, E. Fridell, E. Jobson, and B. Andersson. Induced low temperature catalytic ignition by transient changes in the gas composition. *Catalysis Today* **73**.3-4 (2002), 307–313. DOI: 10.1016/S0920-5861(02)00014-7.
- [26] A. I. Frenkel, S. Khalid, J. C. Hanson, and M. Nachtegaal. “QEXAFS in Catalysis Research: Principles, Data Analysis, and Applications”. *In-situ Characterization of Heterogeneous Catalysts*. Ed. by J. A. Rodriguez, J. C. Hanson, and P. J. Chupas. Hoboken, New Jersey: John Wiley & Sons Inc., 2013, pp. 23–47. DOI: 10.1002/9781118355923.ch1.
- [27] M. A. Newton and A. J. Dent. “Energy-Dispersive EXAFS: Principles and Application in Heterogeneous Catalysis”. *In-situ Characterization of Heterogeneous Catalysts*. Hoboken, New Jersey: John Wiley & Sons Inc., 2013, pp. 75–119. DOI: 10.1002/9781118355923.ch3.
- [28] J. J. Rehr, J. J. Kas, F. D. Vila, M. P. Prange, and K. Jorissen. Parameter-free calculations of X-ray spectra with FEFF9. *Physical chemistry chemical physics : PCCP* **12**.21 (2010), 5503–5513. DOI: 10.1039/b926434e.
- [29] A. L. Ankudinov, B. Ravel, J. J. Rehr, and S. D. Conradson. Real-space multiple-scattering calculation and interpretation of x-ray-absorption near-edge structure. *Physical Review B* **58**.12 (1998), 7565–7576. DOI: 10.1103/PhysRevB.58.7565.
- [30] J. J. Rehr and R. C. Albers. Theoretical approaches to x-ray absorption fine structure. *Reviews of Modern Physics* **72**.3 (2000), 621–654. DOI: 10.1103/RevModPhys.72.621.
- [31] G. Bunker. *Introduction to XAFS*. Cambridge: Cambridge University Press, 2010.
- [32] B. Ravel. A practical introduction to multiple scattering theory. *Journal of Alloys and Compounds* **401**.1-2 (2005), 118–126. DOI: 10.1016/j.jallcom.2005.04.021.
- [33] A. Urakawa, T. Bürgi, and A. Baiker. Sensitivity enhancement and dynamic behavior analysis by modulation excitation spectroscopy: Principle and application in heterogeneous catalysis. *Chemical Engineering Science* **63**.20 (2008), 4902–4909. DOI: 10.1016/j.ces.2007.06.009.
- [34] D. Ferri, M. A. Newton, M. Di Michiel, G. L. Chiarello, S. Yoon, Y. Lu, and J. Andrieux. Revealing the dynamic structure of complex solid catalysts using modulated excitation X-ray diffraction. *Angewandte Chemie International Edition* **53**.34 (2014), 8890–8894. DOI: 10.1002/anie.201403094.
- [35] A. Urakawa, W. Van Beek, M. Monrabal-Capilla, J. R. Galán-Mascarós, L. Palin, and M. Milanesio. Combined, Modulation Enhanced X-ray Powder Diffraction and Raman Spectroscopic Study of Structural Transitions in the Spin Crossover Material [Fe(Htrz)₂(trz)](BF₄). *The Journal of Physical Chemistry C* **2** (2011), 1323–1329. DOI: 10.1021/jp107206n.
- [36] D. Ferri, M. S. Kumar, R. Wirz, A. Eyssler, O. Korsak, P. Hug, A. Weidenkaff, and M. A. Newton. First steps in combining modulation excitation spectroscopy with synchronous dispersive EXAFS/DRIFTS/mass spectrometry for in situ time resolved study of heterogeneous catalysts. *Physical chemistry chemical physics* **12**.21 (2010), 5634–5446. DOI: 10.1039/b926886c.

- [37] D. Ferri, M. A. Newton, and M. Nachtegaal. Modulation Excitation X-Ray Absorption Spectroscopy to Probe Surface Species on Heterogeneous Catalysts. *Topics in Catalysis* **54**.16-18 (2011), 1070–1078. DOI: 10.1007/s11244-011-9727-5.
- [38] D. Baurecht and U. P. Fringeli. Quantitative modulated excitation Fourier transform infrared spectroscopy. *Review of Scientific Instruments* **72**.10 (2001), 3782. DOI: 10.1063/1.1400152.
- [39] M. V. Twigg. Catalytic control of emissions from cars. *Catalysis Today* **163**.1 (2011), 33–41. DOI: 10.1016/j.cattod.2010.12.044.
- [40] J. Wang, H. Chen, Z. Hu, M. Yao, and Y. Li. A Review on the Pd-Based Three-Way Catalyst. *Catalysis Reviews: Science and Engineering* **57**.1 (2015), 79–144. DOI: 10.1080/01614940.2014.977059.
- [41] M. Ozawa. Role of cerium–zirconium mixed oxides as catalysts for car pollution: A short review. *Journal of Alloys and Compounds* **275-277** (1998), 886–890. DOI: 10.1016/S0925-8388(98)00477-0.
- [42] A. Papavasiliou, A. Tsetsekou, V. Matsouka, M. Konsolakis, I. Yentekakis, and N. Boukos. Development of a Ce–Zr–La modified Pt/ γ -Al₂O₃ TWCs’ washcoat: Effect of synthesis procedure on catalytic behaviour and thermal durability. *Applied Catalysis B: Environmental* **90**.1-2 (2009), 162–174. DOI: 10.1016/j.apcatb.2009.03.006.
- [43] J. R. H. Ross. *Heterogeneous catalysis fundamentals and applications*. Elsevier, 2012.
- [44] A. Stierle. Oxidation of palladium: from single crystal surfaces towards nanoparticles. *International Journal of Materials Research* **100**.10 (2009), 1308–1317. DOI: 10.3139/146.110200.
- [45] C. J. Heard, S. Vajda, and R. L. Johnston. Support and oxidation effects on subnanometer palladium nanoparticles. *Journal of Physical Chemistry C* **118**.7 (2014), 3581–3589. DOI: 10.1021/jp411019t.
- [46] J. A. Anderson, M. Fernández-García, and A. Martínez-Arias. “Determination of dispersion and crystallite sizes for supported metal catalysts”. *Supported Metals in Catalysis*. Ed. by J. A. Anderson and M. Fernández-García. 2nd ed. London: Imperial Collage Press, 2012.
- [47] H. Niehus, W. Heiland, and E. Taglauer. Low-energy ion scattering at surfaces. *Surface Science Reports* **17**.4-5 (1993), 213–303. DOI: 10.1016/0167-5729(93)90024-J.
- [48] R. J. Farrauto. Low-Temperature Oxidation of Methane. *Science* **337**.6095 (2012), 659–660. DOI: 10.1126/science.1226310.
- [49] E. Becker, P.-A. Carlsson, H. Grönbeck, and M. Skoglundh. Methane oxidation over alumina supported platinum investigated by time-resolved in situ XANES spectroscopy. *Journal of Catalysis* **252**.1 (2007), 11–17. DOI: 10.1016/j.jcat.2007.09.004.
- [50] E. Becker, P.-A. Carlsson, L. Kylhammar, M. A. Newton, and M. Skoglundh. In Situ Spectroscopic Investigation of Low-Temperature Oxidation of Methane over Alumina-Supported Platinum during Periodic Operation. *The Journal of Physical Chemistry C* **115**.4 (2011), 944–951. DOI: 10.1021/jp103609n.

- [51] R. F. Hicks, H. Qi, M. L. Young, and R. G. Lee. Structure sensitivity of methane oxidation over platinum and palladium. *Journal of Catalysis* **122.2** (1990), 280–294. DOI: 10.1016/0021-9517(90)90282-0.
- [52] M. Lyubovsky and L. Pfefferle. Complete methane oxidation over Pd catalyst supported on α -alumina. Influence of temperature and oxygen pressure on the catalyst activity. *Catalysis Today* **47.1-4** (1999), 29–44. DOI: 10.1016/S0920-5861(98)00281-8.
- [53] S. H. Oh, P. J. Mitchell, and R. M. Siewert. Methane oxidation over alumina-supported noble metal catalysts with and without cerium additives. *Journal of Catalysis* **132.2** (1991), 287–301. DOI: 10.1016/0021-9517(91)90149-X.
- [54] R. Burch, P. K. Loader, and F. J. Urbano. Some aspects of hydrocarbon activation on platinum group metal combustion catalysts. *Catalysis Today* **27.1-2** (1996), 243–248. DOI: 10.1016/0920-5861(95)00194-8.
- [55] J. G. McCarty. Kinetics of PdO combustion catalysis. *Catalysis Today* **26.3-4** (1995), 283–293. DOI: 10.1016/0920-5861(95)00150-7.
- [56] A. Hellman, A. Resta, N. M. Martin, J. Gustafson, A. Trinchero, P.-A. Carlsson, O. Balmes, R. Felici, R. van Rijn, J. W. M. Frenken, J. N. Andersen, E. Lundgren, and H. Grönbeck. The Active Phase of Palladium during Methane Oxidation. *Journal of Physical Chemistry Letters* **3.6** (2012), 678–682. DOI: 10.1021/jz300069s.
- [57] N. M. Martin, M. Van den Bossche, A. Hellman, H. Grönbeck, C. Hakanoglu, J. Gustafson, S. Blomberg, N. Johansson, Z. Liu, S. Axnanda, J. F. Weaver, and E. Lundgren. Intrinsic Ligand Effect Governing the Catalytic Activity of Pd Oxide Thin Films. *ACS Catalysis* **4.10** (2014), 3330–3334. DOI: 10.1021/cs5010163.
- [58] M. Van den Bossche and H. Grönbeck. Methane Oxidation over PdO(101) Revealed by First-Principles Kinetic Modeling. *Journal of the American Chemical Society* **137.37** (2015), 12035–12044. DOI: 10.1021/jacs.5b06069.
- [59] S. K. Matam, M. H. Aguirre, A. Weidenkaff, and D. Ferri. Revisiting the Problem of Active Sites for Methane Combustion on Pd/Al₂O₃ by Operando XANES in a Lab-Scale Fixed-Bed Reactor. *The Journal of Physical Chemistry C* **114.20** (2010), 9439–9443. DOI: 10.1021/jp1019697.
- [60] X. Weng, H. Ren, M.-s. Chen, and H. Wan. Effect of Surface Oxygen on the Activation of Methane on Palladium and Platinum Surfaces. *ACS Catalysis* **4.8** (2014), 2598–2604. DOI: 10.1021/cs500510x.
- [61] Y. Lu, M. Santhosh Kumar, G. L. Chiarello, P. Dimopoulos Eggenschwiler, C. Bach, M. Weilenmann, A. Spiteri, A. Weidenkaff, and D. Ferri. Operando XANES study of simulated transient cycles on a Pd-only three-way catalyst. *Catalysis Communications* **39** (2013), 55–59. DOI: 10.1016/j.catcom.2013.05.006.
- [62] Y. Lu, S. Keav, V. Marchionni, G. L. Chiarello, A. Pappacena, M. Di Michiel, M. A. Newton, A. Weidenkaff, and D. Ferri. Ageing induced improvement of methane oxidation activity of Pd/YFeO₃. *Catalysis Science & Technology* **4.9** (2014), 2919. DOI: 10.1039/C4CY00289J.
- [63] R. Burch, F. J. Urbano, and P. K. Loader. Methane combustion over palladium catalysts: The effect of carbon dioxide and water on activity. *Applied Catalysis A: General* **123.1** (1995), 173–184. DOI: 10.1016/0926-860X(94)00251-7.

- [64] D. Ciuparu, N. Katsikis, and L. Pfefferle. Temperature and time dependence of the water inhibition effect on supported palladium catalyst for methane combustion. *Applied Catalysis A: General* **216**.1-2 (2001), 209–215. DOI: 10.1016/S0926-860X(01)00558-0.
- [65] S. C. Su, J. N. Carstens, and A. T. Bell. A Study of the Dynamics of Pd Oxidation and PdO Reduction by H₂ and CH₄. *Journal of Catalysis* **176**.1 (1998), 125–135. DOI: 10.1006/jcat.1998.2028.
- [66] Y.-H. C. Chin, C. Buda, M. Neurock, and E. Iglesia. Consequences of metal-oxide interconversion for C–H bond activation during CH₄ reactions on Pd catalysts. *Journal of the American Chemical Society* **135**.41 (2013), 15425–42. DOI: 10.1021/ja405004m.
- [67] C. Bozo, N. Guilhaume, and J.-M. Herrmann. Role of the Ceria–Zirconia Support in the Reactivity of Platinum and Palladium Catalysts for Methane Total Oxidation under Lean Conditions. *Journal of Catalysis* **203**.2 (2001), 393–406. DOI: 10.1006/jcat.2001.3320.
- [68] M. Haneda, T. Mizushima, and N. Kakuta. Synergistic Effect between Pd and Nonstoichiometric Cerium Oxide for Oxygen Activation in Methane Oxidation. *The Journal of Physical Chemistry B* **102**.34 (1998), 6579–6587. DOI: 10.1021/jp9819285.
- [69] K. Narui, H. Yata, K. Furuta, A. Nishida, Y. Kohtoku, and T. Matsuzaki. Effects of addition of Pt to PdO/Al₂O₃ catalyst on catalytic activity for methane combustion and TEM observations of supported particles. *Applied Catalysis A: General* **179**.1-2 (1999), 165–173. DOI: 10.1016/S0926-860X(98)00306-8.
- [70] G. Lapisardi, L. Urfels, P. G lin, M. Primet, A. Kaddouri, E. Garbowski, S. Toppi, and E. Tena. Superior catalytic behaviour of Pt-doped Pd catalysts in the complete oxidation of methane at low temperature. *Catalysis Today* **117**.4 (2006), 564–568. DOI: 10.1016/j.cattod.2006.06.004.
- [71] K. Persson, A. Ersson, K. Jansson, J. L. Fierro, and S. G. J r s. Influence of molar ratio on Pd-Pt catalysts for methane combustion. *Journal of Catalysis* **243**.1 (2006), 14–24. DOI: 10.1016/j.jcat.2006.06.019.
- [72] R. Strobel, J. D. Grunwaldt, A. Camenzind, S. E. Pratsinis, and A. Baiker. Flame-made alumina supported Pd-Pt nanoparticles: Structural properties and catalytic behavior in methane combustion. *Catalysis Letters* **104**.1-2 (2005), 9–16. DOI: 10.1007/s10562-005-7429-y.
- [73] M. Chen and L. D. Schmidt. Morphology and composition of Pt–Pd alloy crystallites on SiO₂ in reactive atmospheres. *Journal of Catalysis* **56**.2 (1979), 198–218. DOI: 10.1016/0021-9517(79)90107-6.
- [74] L. C. A. van den Oetelaar, O. W. Nooij, S. Oerlemans, A. W. Denier van der Gon, H. H. Brongersma, L. Lefferts, A. G. Roosenbrand, and J. A. R. van Veen. Surface Segregation in Supported Pd-Pt Nanoclusters and Alloys. *The Journal of Physical Chemistry B* **102**.18 (1998), 3445–3455. DOI: 10.1021/jp973395q.
- [75] P. L. Hansen, A. M. Molenbroek, and A. V. Ruban. Alloy Formation and Surface Segregation in Zeolite-Supported Pt-Pd Bimetallic Catalysts. *Journal of Physical Chemistry B* **101**.96 (1997), 1861–1868. DOI: 10.1021/jp962771o.

- [76] K. Persson, K. Jansson, and S. G. Järås. Characterisation and microstructure of Pd and bimetallic Pd-Pt catalysts during methane oxidation. *Journal of Catalysis* **245.2** (2007), 401–414. DOI: 10.1016/j.jcat.2006.10.029.
- [77] N. M. Martin, J. Nilsson, M. Skoglundh, E. C. Adams, X. Wang, P. Velin, G. Smedler, A. Raj, D. Thompsett, H. H. Brongersma, T. Grehl, G. Agostini, O. Mathon, S. Carlson, K. Norén, F. J. Martinez-Casado, Z. Matej, O. Balmes, and P.-A. Carlsson. Characterization of Surface Structure and Oxidation/Reduction Behavior of Pd–Pt/Al₂O₃ Model Catalysts. *The Journal of Physical Chemistry C* **120.49** (2016), 28009–28020. DOI: 10.1021/acs.jpcc.6b09223.